# Stilbenoid Dimers: Dissection of a Paracyclophane Chromophore

**Guillermo C. Bazan,\*,† Warren J. Oldham, Jr.,‡ Rene J. Lachicotte,‡ Sergei Tretiak,§ Vladimir Chernyak,§ and Shaul Mukamel\*,§**

*Contribution from the Department of Chemistry, University of Rochester, Rochester, New York 14627, Department of Chemistry, University of California, Santa Barbara, California 93106, and Department of Chemistry and Rochester Theory Center for Optical Science and Engineering, University of Rochester, Rochester, New York 14627*

*Received November 5, 1997*

**Abstract:** A series of paracyclophane derivatives that hold chromophores of varying conjugation lengths has been synthesized using palladium-mediated coupling reactions. These molecules mimic solid-state interactions in main-chain polychromophores and conjugated emissive polymers such as poly(*p*-phenylenevinylene) (PPV). Their optical properties give insight into the energetics of photoexcitations localized in a discrete chromophore relative to a state containing the through-space delocalized paracyclophane core. Thus, 4-vinyl[2.2]-paracyclophane (**5**) is obtained by reaction of 4-bromo[2.2]paracyclophane (**3**) and ethylene using Pd(OAc)$_2$ and P(*o*-tol)$_3$. Similar reactions starting with pseudo-*o*- or pseudo-*p*-dibromo[2.2]paracyclophane (**4a** and **4b**, respectively) give the pseudo-*o*- and pseudo-*p*-divinyl products (**6a** and **6b**, respectively). Using styrene instead of ethylene provides the styryl-substituted products. Thus, 4-styryl[2.2]paracyclophane (**7**) is obtained from **3** while pseudo-*p*- and pseudo-*o*-distyryl[2.2]paracyclophane (**1a** and **1b**) are obtained from **4a** and **4b**, respectively. Compounds **1a** and **1b** can be viewed as stilbene dimers that have a pair of cofacial arene units at a fixed distance. Pseudo-*p*-bis(4-vinyl-styryl)[2.2]paracyclophane (**9**) was prepared by reaction of CH$_2$-PPh$_3$ with pseudo-*p*-bis(4-carboxaldehyde-styryl)[2.2]paracyclophane. Reacting 4-(4-*tert*-butylstyryl)styrene with **3**, **4a**, or **4b** under Heck-type conditions gives 4-[4-(4-*tert*-butylstyryl)styryl][2.2]paracyclophane (**10**) and pseudo-*p*- and pseudo-*o*-bis[4-(4-*tert*-butylstyryl)styryl][2.2]paracyclophane(**2a** and **2b**), respectively. The observed trends in absorption, fluorescence and radiative lifetime of these compounds are reported and analyzed using collective electronic oscillators (CEO) representing the changes induced in the reduced single-electronic density matrix upon optical excitation. Comparison of the CEO of the aggregates with the corresponding monomers using two-dimensional plots provides an efficient method for tracing the origin of the various optical transitions by identifying the underlying changes in charge densities and bond orders. For **5**, **6a,b**, **7**, and **1a,b** the emission is red-shifted from the "monomeric" compound and featureless, reminiscent of excimer qualities. The emissions of **9**, **10**, and **2a,b** are similar to the "monomer" and display vibronic structure. Thus, for the smaller chromophores, emission occurs from a state containing the through-space delocalized paracyclophane core. In the situation where extended chromophores, with more stable excited states, are held together with the paracyclophane core, the photophysics of the individual chromophores dominates. The present analysis is relevant to the design and synthesis of organic molecules with desired optical properties.

## Introduction

The optical response of chromophore aggregates provides an important tool in the studies of intermolecular interactions and bonding. Extensive experimental and theoretical attention has been devoted to studies of clusters in supersonic beams,[1,2] J-aggregates of cyanine dyes,[3] supramolecular structures,[4] and biological complexes (photosynthetic antennae and reaction centers).[5] It is possible to treat the aggregates as giant molecules and employ methods of quantum chemistry to calculate their electronic structure. These approaches are limited to small aggregates.[6,7] An important challenging goal of computational chemistry is to relate the electronic states and spectra of aggregates to those of their basic building blocks—the monomers. By doing so it should become possible to get a better

† Department of Chemistry, University of California, Santa Barbara.

‡ Department of Chemistry, University of Rochester.

§ Department of Chemistry and Rochester Theory Center for Optical Science and Engineering, University of Rochester.

(1) (a) Easter, D. C.; Whetten, R. L.; Wessel, J. E. *J. Chem. Phys.* **1991**, *94*, 3347. (b) Easter, D. C.; Khoury, J. T.; Whetten, R. L. *J. Chem. Phys.* **1992**, *97*, 1675. (c) Easter, D. C.; Baronavski, A. P.; Whetten, R. L. *J. Chem. Phys.* **1993**, *99*, 4942.

(2) (a) Syage, J. A.; Wessel, J. E. *J. Chem. Phys.* **1988**, *89*, 5962. (b) Wessel, J. E.; Syage, J. A. *J. Phys. Chem.* **1990**, *94*, 737.

(3) (Special Issue, *Confined Excitations in Molecular and Semiconductor Nanostructures*; Mukamel, S., Chemla, D. S., Eds.) *Chem. Phys.* **1996**, 210.

(4) (a) Berberan-Santos, M. N.; Canceill, J.; Brochon, J.-C.; Jullien, L.; Lehn, J.-M.; Pouget, J.; Tauc, P.; Valeur, B. *J. Am. Chem. Soc.* **1992**, *114*, 6427. (b) Berberan-Santos, M. N.; Pouget, J.; Tauc, P.; Valeur, B.; Canceill, J.; Jullien, L.; Lehn, J.-M. *J. Phys. Chem.* **1993**, *97*, 11376. (c) Berberan-Santos, M. N.; Canceill, J.; Gratton, E.; Jullien, L.; Lehn, J.-M.; So, J.; Sutin, J.; Valeur, B. *J. Phys. Chem.* **1996**, *100*, 15.

(5) *Special Issue on Light-Harvesting Physics Workshop*; *J. Phys. Chem. B* **1997**, 101. Sundström, V.; van Grondelle, R. In *Anoxygenic Photosynthetic Bacteria*; Blankenship, R. E., Madiga, M. T., Baner, C. E., Eds.; Kluver Academic: Dordrecht, 1995; p 349.

(6) (a) Scholes, G. D.; Ghiggino, K. P.; Oliver, A. M.; Paddon-Row, M. N. *J. Am. Chem. Soc.* **1993**, *115*, 4345. (b) Clayton, A. H. A.; Scholes, G. D.; Ghiggino, K. P.; Paddon-Row, M. N. *J. Phys. Chem.* **1996**, *100*, 10912.

(7) (a) Hobza, P.; Selzle, H. L.; Schlag, E. W. *J. Am. Chem. Soc.* **1994**, *116*, 3500. (b) Börsen, K. O.; Lin, S. H.; Selzle, H. L.; Schlag, E. W. *J. Chem. Phys.* **1989**, *90*, 1299. (c) Cársky, P.; Selzle, H. L.; Schlag, E. W. *Chem. Phys.* **1988**, *125*, 165.

*Stilbenoid Dimers*

*J. Am. Chem. Soc., Vol. 120, No. 36, 1998* 9189

microscopic insight into the nature of their electronic excitations and to predict qualitative features of complex large systems using simple, readily available information.

It is clear that the spatial relationship between polymer chains controls to a significant extent important photooptic and electrooptic properties, such as emission quantum yield and charge transport ability, in emissive polymers.[8,9] Morphological irregularities and the statistical nature of chain lengths and conjugation lengths, combine with facile energy-transfer processes to make experimental probing of aggregated sites difficult. Despite the importance of these interactions, well-defined monomolecular models suitable for studying intermolecular effects in the amorphous solid state are generally lacking.

In this paper we report the photophysics of a family of paracyclophane derivatives that hold phenylenevinylene units of varying complexity. The optical properties of these dimers are analyzed using the recently developed collective electronic oscillator (CEO) approach.[10−13]

Compounds containing the [2.2]paracyclophane core[14] were chosen because they have proven valuable in the inquiry of bonding, ring strain, and $\pi-\pi$ electron delocalization in organic molecules.[15] It is possible with this framework to hold chromophores in close proximity and to enforce cofacial overlap of two arene rings. Examination of the photooptical properties of this class of compounds has given insight into the effect of through-space delocalization for a pair of chromophores in a precisely determined distance and orientation. For example, [2.2]paracyclophane (**Pc**) behaves as a pair of strongly interact-

(Pc)
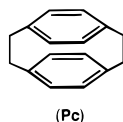
ing benzene rings and displays spectroscopic features which have been described as analogous to those of a benzene excimer.[16] Bichromophoric dimers containing a [2.2]cyclophane locus can therefore model interchromophore contacts in the solid state.[17,18]

The synthesis and spectroscopic properties of the pseudo-*ortho* and pseudo-*para* isomers of distyryl[2.2]paracyclophane (**1a** and **1b**) and bis[4-(4′-*tert*-butylstyryl)styryl][2.2]paracyclophane (**2a** and **2b**) was recently reported.[19]

These molecules represent dimers of stilbene and distyrylbenzene and are interesting in that they model interchromophore contacts in main-chain polychromophores such as poly(para-cyclophan-1-ene)[20] and conjugated polymers such as poly(*p*-phenylenevinylene) (PPV).

(PPV)

A question of fundamental importance for molecules such as **2a,b** concerns the extent of delocalization for the inter-ring state, since it plays an important role in determining the frequency and efficiency of emission and because it reflects the ability of closely spaced fragments to delocalize through space. It is not clear how the energy of this state is stabilized by pendant conjugated fragments or how this energy compares relative to an excitation localized on a single chromophore.

In this paper we dissect molecules **2a** and **2b** in order to determine the relative energies of the state and the excited-state localized on a single chromophore. The optical properties of **1a,b** and **2a,b** and their relationship to those of **Pc** are understood on the basis of the CEO approach.

## Results and Discussion

**Syntheses and Characterization.** Derivatization of **Pc** is accomplished via electrophilic bromination as originally described by Reich and Cram.[21] Reactions carried out using 1 equiv of bromine yield monobromo[2.2]paracyclophane (**3**) in high yield. However, reactions carried out using 2 equiv of bromine are known to give a mixture of four dibromo[2.2]-paracyclophane isomers. Because the pseudo-*p*-dibromo-

(8) A concise review on excimer formation and luminescence in conjugated polymers can be found in: Conwell, E. *Trends Polym. Sci.* **1997**, *5*, 218. See also: Cornil, J.; dos Santos, D. A.; Crispin, X.; Silbey, R.; Bredas, J. L. *J. Am. Chem. Soc.* **1998**, *120*, 1289−1299.

(9) (a) Lee, C. H.; Yu, G.; Moses, D.; Heeger, A. J. *Synth. Met.* **1995**, *69* (1−3), 429. (b) Gettinger, C. L.; Heeger, A. J.; Drake, J. M.; Pine, D. J. J. *Chem. Phys.* **1994**, *101*, 1673. (c) Kohler, A.; Gruner, J.; Friend, R. H.; Mullen, K.; Scherf, U. *Chem. Phys. Lett.* **1995**, *243*, 456.

(10) (a) Takahashi, A.; Mukamel, S. *J. Chem. Phys.* **1994**, *100*, 2366. (b) Mukamel, S.; Takahashi, A.; Wang, H. X.; Chen, G. *Science* **1994**, *266*, 250. (c) Chernyak, V.; Mukamel. S. *J. Chem. Phys.* **1996**, *104*, 444.

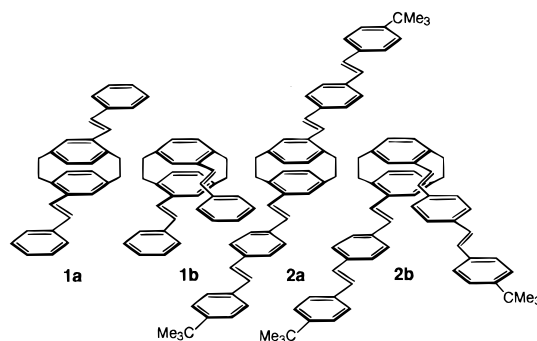(11) Mukamel, S.; Tretiak, S.; Wagersreiter, T.; Chernyak, V. *Science* **1997**, *277*, 781.

(12) (a) Tretiak, S.; Chernyak, V.; Mukamel, S. *Chem. Phys. Lett.* **1996**, *259*, 55. (b) Tretiak, S.; Chernyak, V.; Mukamel, S. *J. Chem. Phys.* **1996**, *105*, 8914.

(13) (a) Tretiak, S.; Chernyak, V.; Mukamel, S. *J. Am. Chem. Soc.* **1997**, *119*, 11408. (b) Tretiak, S.; Chernyak, V.; Mukamel, S. *J. Phys. Chem. B* **1998**, *102*, 3310.
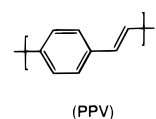
(14) Cram, D. J.; Bauer, R. H. *J. Am. Chem. Soc.* **1959**, *81*, 5971.

(15) Voegtle, F. *Cyclophane Chemistry*; J. Wiley & Sons: New York, 1993.

(16) Birks, B. J. *Photophysics of Aromatic Molecules*; Wiley-Interscience: London, 1970.

(17) Other chromophores studied in this manner include: (a, phenanthrenophane) Schweitzer, D.; Hausser, K. H.; Haenel, M. W. *Chem. Phys.* **1978**, *29*, 181. (b, anthracenophane) Ishikawa, S.; Nakamura, J.; Iwata, S.; Sumitami, M.; Nagakura, S.; Sakata, Y.; Misumi, S. *Bull. Chem. Soc. Jpn.* **1979**, *52*, 1346. (c, fluorenophane) Haenel, M. W. *Tetrahedron Lett.* **1976**, *36*, 3121. Colpa, J. P.; Hausser K. H.; Schweitzer, D. *Chem. Phys.* **1978**, *29*, 187. (d, pyrenophane and several isomers of naphthalenophane) Haenel, M.; Staab, H. A. *Chem. Ber.* **1973**, *106*, 2203. Otsubo, T.; Mizogami, S.; Osaka, N.; Sakata, Y.; Misumi, S. *Bull. Chem. Soc. Jpn.* **1977**, *50*, 1858. For studies of cycloaddition reactions, see: (e) Grieving, H.; Hopf, H.; Jones, P. G.; Bubenitscheck, P.; Desvergne, J. P.; Bouass-Laurent, H. *J. Chem. Soc., Chem. Commun.* **1994**, 1075. (f) Okada, Y.; Ishii, F.; Akiyama, I.; Nishimura, J. *Chem. Lett.* **1992**, 1579. (g) Grieving, H.; Hopf, H.; Jones, P. G.; Bubenitscheck, P.; Desvergne, J. P.; Bouass-Laurent, H. *Liebigs. Ann.* **1995**, 1949.

(18) Doris, K. A.; Ellis, D. E.; Ratner, M. A.; Marks, T. J. *J. Am. Chem. Soc.* **1984**, *106*, 2491.

(19) Oldham, W. J., Jr.; Miao, Y.-J.; Lachicotte, R. J.; Bazan, G. C. *J. Am. Chem. Soc.* **1998**, *120*, 419.

(20) Miao, Y.-J.; Herkstroeter, W. G.; Sun, B. J.; Wong-Foy, A. G.; Bazan, G. C. *J. Am. Chem. Soc.* **1995**, *117*, 11407.

(21) Reich, H. J.; Cram, D. J. *J. Am. Chem. Soc.* **1969**, *91*, 3527. See also: Izuoka, A.; Murata, S.; Sugawara, T.; Iwamura, H, *J. Am. Chem. Soc.* **1987**, *109*, 2631.
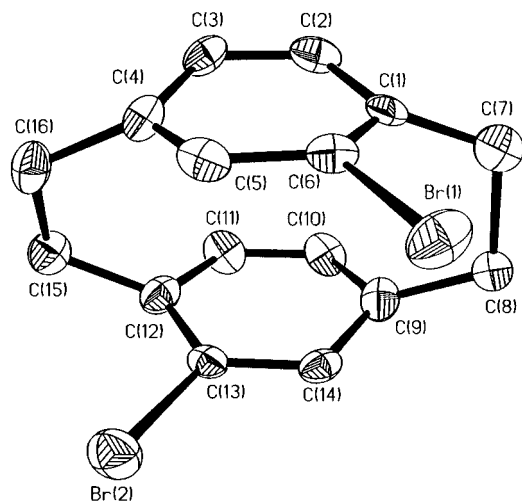
**Figure 1.** ORTEP drawing of **4b** at 30% probability. Hydrogen atoms are not shown.

[2.2]paracyclophane, **4a**, and the pseudo-*o*-dibromo[2.2]-paracyclophane, **4b**, isomers can be obtained in reasonable yields, we have chosen these as suitable starting materials. Due to its poor solubility, **4a** can be obtained in pure form upon recrystallization of the crude product mixture from a warm solution of chloroform and hexanes. The filtrate following recrystallization may then be subjected to column chromatography (silica, hexanes) to obtain **4b** which is the most polar of the dibromo isomers and elutes last from the column.
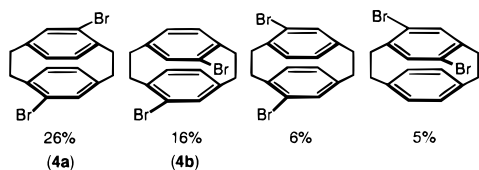


More recently, de Meijere and co-workers have described a solid-phase bromination of **Pc** using bromine vapor to obtain **4b** following purification by column chromatography.[22] However, spectroscopic characterization of this material is identical to published values reported for **4a**.[23] Given the uncertainty in isomer assignment, we considered it prudent to independently confirm the structure of **4b**. High-quality single crystals of **4b** were obtained upon slow diffusion of hexanes into a concentrated CHCl$_3$ solution. As shown in Figure 1, this experiment unambiguously confirms Cram's original characterization. Metrical data obtained for **4b** are very similar to published values for related [2.2]paracyclophane compounds.[24] The bond lengths and angles obtained for **4b** are similar to values reported for the pseudo-*para* isomer, **4a**, except that the inter-ring torsion angle in the pseudo-*ortho* isomer is significantly larger, presumably to minimize steric interactions between the two large bromine atoms (C1−C7−C8−C9 = 19.0° vs 5.8° in the pseudo-*para* isomer).[25]

A variety of stilbenoid derivatives incorporating the **Pc** core can be prepared from the appropriate bromo-paracyclophane derivatives using standard Heck coupling procedures. Monovinyl-[2.2]paracyclophane, **5** is obtained in 85% yield upon heating a dimethylformamide solution of **3** sealed in a high-pressure steel bomb under ethylene (100 psi) and in the presence of excess NEt$_3$ and a catalytic mixture of Pd(OAc)$_2$ and P(*o*-tol)$_3$ (*o*-tol = *o*-tolyl, see eq 1).

(22) König, B.; Knieriem, B.; de Meijere, A. *Chem. Ber.* **1993**, *126*, 1643.
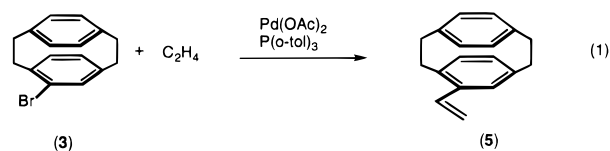


A similar procedure carried out using the dibromo[2.2]-paracyclophane compounds, **4a** and **4b** provides the corresponding divinyl derivatives, pseudo-*p*-divinyl[2.2]paracyclophane, **6a**, and pseudo-*o*-divinyl[2.2]paracyclophane, **6b**, respectively in yields greater than 90% (eq 2). Compounds **5** and **6a** are
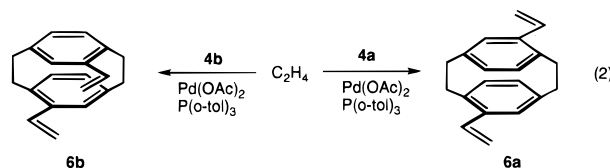


known in the literature; however, to our knowledge synthetic details have not been published in the case of **6a**.[26] The monovinyl derivative was previously prepared in three steps by Friedel−Crafts acylation of **Pc**, followed by reduction of the acetyl intermediate to the corresponding alcohol and thermal dehydration.[27] The Heck coupling procedure offers advantages in terms of synthetic ease and improved yields.

Palladium-mediated coupling of styrene with the appropriate bromoparacyclophane derivatives provides an efficient route to the corresponding styrylcyclophane compounds. While the traditional Heck catalyst system[28] composed of a mixture of Pd(OAc)$_2$ and P(*o*-tol)$_3$ is effective for this reaction, isolated yields are typically less than 50%. Improved yields are obtained for the phase-transfer catalyst system developed by Jeffery, composed of a mixture of Pd(OAc)$_2$ with excess K$_2$CO$_3$ and NBu$_4$Br.[29] In fact, this synthetic procedure has been previously employed by de Meijere and co-workers in the synthesis of styryl[2.2]paracyclophane (**7**) from **3**.[22] Wittig chemistry has also proven useful in the preparation of compounds of this type.[30]
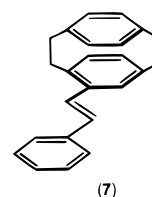


Extension of this reactivity to compounds **4a** and **4b** gives the pseudo-*p*-distyryl[2.2]paracyclophane, **1a**, and pseudo-*o*-distyryl[2.2]paracyclophane, **1b**, as shown in eq 3. These are highly crystalline materials which have been structurally

(23) Reich, H. J.; Cram, D. J. *J. Am. Chem. Soc.* **1969**, *91*, 3534.

(24) Keehn, P. M. In *Cyclophanes*; Keehn, P. M., Rosenfeld, S. M., Eds.; Academic Press: New York, 1983; Vol 1, pp 69−238.

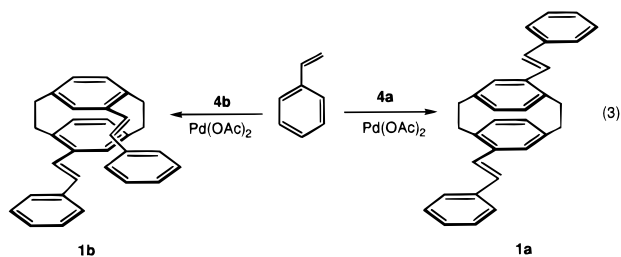(25) Lindeman, S. V.; Struchkov, Y. T.; Guryshev, V. N. *Bull. Acad. Sci. USSR* **1986**, *35*, 1825.

(26) (a) Yang, Z.-z.; Heilbronner, E.; Hopf, H.; Ehrhardt, S.; Hentschel, S. *J. Phys. Chem.* **1988**, *92*, 914. (b) Gollas, B.; Speiser, B.; Sieglen, J.; Strähle, J. *Organometallics* **1996**, *15*, 260.

(27) Iwatsuki, S.; Itoh, T.; Kubo, M.; Okuno, H. *Polym. Bull.* **1994**, *32*, 27.

(28) Heck, R. F. *Org. React.* **1982**, *27*, 345.

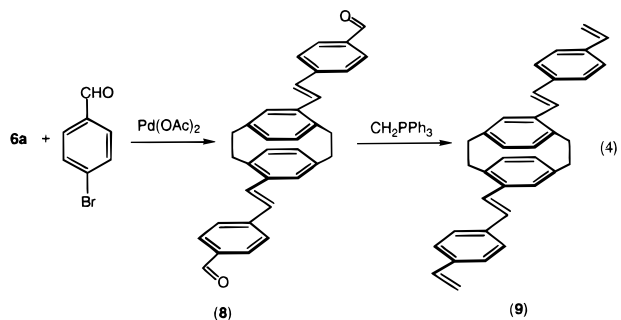(29) Jeffery, T. *Adv. Met.-Org. Chem.* **1996**, *5*, 153.

(30) (a) Schenk, R.; Gregorius, H.; Meerholz, K.; Heinze, J.; Müllen, K, *J. Am. Chem. Soc.* **1991**, *113*, 2634. (b) Hopf, H,; Mlynek, C.; El-Tamany, S.; Ernst, L. *J. Am. Chem. Soc.* **1985**, *107*, 6620.

**Figure 2.** ORTEP drawing of **7** at 30% probability. Hydrogen atoms are not shown.

characterized previously and are easily purified by chromatography. Blue emission from both compounds is readily apparent to the eye.

Crystals suitable for X-ray structural analysis have been obtained for **7** by allowing a hexane solution to slowly evaporate and an ORTEP diagram is shown in Figure 2. The bond lengths and angles observed for the cyclophane portion of **7** are similar to **Pc**, in keeping with the rigid nature of this structural unit. Other than puckering of one of the arenes (cyclophane portion), the bond lengths and angles which define a *trans*-stilbene unit in **7** are very similar to *trans*-stilbene itself.[31] For example, *trans*-stilbene is approximately planar with a small torsion angle of 5.2° between the plane of a benzene ring and the alkene portion of the molecule. In comparison the related torsion angles in **7** are −6.08(22)° (C15−C16−C17−C18) and 6.73-(15)° (C20−C19−C18−C17). The respective C=C bond lengths are also quite similar, (1.326(2) in **7** versus an average value for *trans*-stilbene of 1.336(10)) as are the angles around the alkene carbons (C18−C17−C16 = 127.28(14) and C17−C18−C19 = 127.20(14) compared to 126.0 in *trans*-stilbene). The essentially unperturbed stilbene structure that is observed for **7** is mirrored in the structural data that have been previously communicated for **1a** and **1b**, which also reveal unremarkable structural parameters with respect to *trans*-stilbene.

The conjugation length of the stilbenoid compounds considered here can be extended by one additional vinyl unit relative to **1a**. A convenient approach is to couple 4-bromobenzaldehyde with the divinyl derivative, **6a** to give pseudo-*p*-bis(4-carboxaldehydestyryl)[2.2]paracyclophane, **8**. Treatment of **8** with CH$_2$PPh$_3$ yields the desired pseudo-*p*-bis(4-vinylstyryl)-[2.2]paracyclophane, **9** (eq 4).

of TBSS to **3** in the presence of Pd(OAc)$_2$ results in the formation of **10** as shown in eq 5.



Two equivalents of TBSS can be coupled with **4a** or **4b** to give compounds **2a** and **2b** in moderate yields (eq 6). These





are bright fluorescent yellow compounds that are soluble in aromatic, aliphatic, and halogenated solvents. The nonlinear disposition of substituents makes **2b** more soluble than **2a**. In general, all pseudo-*ortho* isomers are more soluble than their pseudo-*para* counterparts.

$^1$H and $^{13}$C NMR spectroscopy provide unambiguous proof of structure for all new compounds. For example, the mono-substituted compounds **5**, **7**, and **10** are chiral which results in four methylene resonances in the $^{13}$C NMR spectra. Disubstitution results in higher symmetry and greatly simplified spectra. Figure 3 shows the $^1$H NMR spectra for the series of pseudo-*para* isomers **6a**, **1a**, **10**, and **2a**.

**Photooptical Properties.** This section describes the absorption and emission spectra of the molecules described above. In some cases the photooptical properties of the paracyclophane dimer are compared with those of compounds which serve as monomer models. Overall, the collected body of data, summarized in Table 1, highlights the effect of delocalization and

Vinylstilbene units can be reacted with **3**, **4a**, or **4b** to provide distyrylbenzenoid-type compounds. The requisite 4-(4-*tert*-butylstyryl)styrene (TBSS) units are obtained by dropwise addition of LiOEt (1 M in EtOH) to an Et$_2$O slurry/solution of 4-vinylbenzylphosphonium chloride and 4-*tert*-butylbenzaldehyde. Although this procedure gives a mixture of both *cis*- and *trans*-stilbene isomers, the former can be isomerized quantitatively to the desired *trans* isomer upon heating a dilute hexane solution with a few crystals of iodine for several hours. Addition
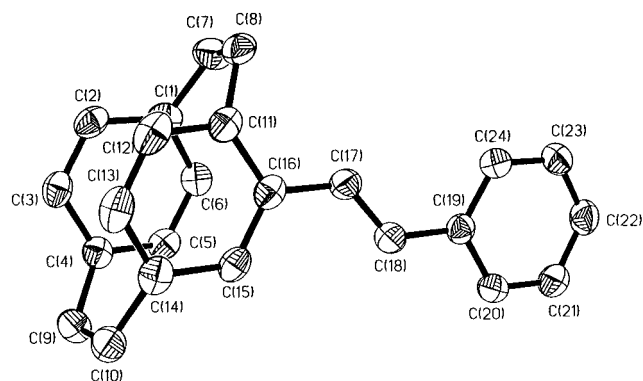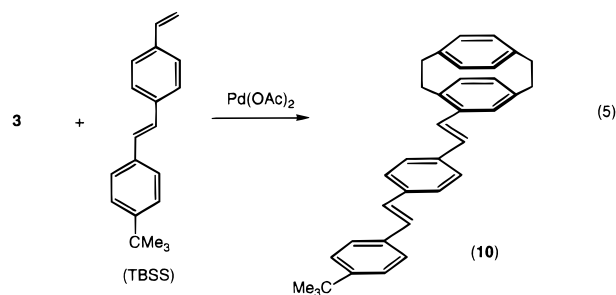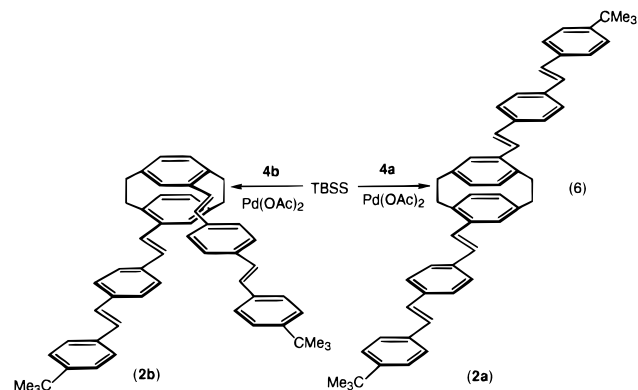
(31) Hoekstra, A.; Meertens, P.; Vos, A. *Acta Crystallogr.* **1975**, *B31*, 2813.

**Table 1.** Summary of Absorption and Emission Data[a]

| | $\lambda_{max}$ | |
| compound | absorption | emission[b] |
| --- | --- | --- |
| **5** | 281 | 374 |
| **6a** | 254 | 394 |
| **6b** | 288 | 386 |
| **7** | 318 | 386 |
| **1a** | 307 | 412 |
| **1b** | 264, 325[c] | 401 |
| **1c** | 294 | 338, 355 |
| **9** | 338 | 390, 409 |
| **10** | 366 | 403, 427 |
| **2a** | 369 | 307, 430 |
| **2b** | 355 | 408, 431 |
| **2c** | 349 | 391, 355 |

[a] All measurements in hexane at room temperature. [b] For emission with vibronic structure the two highest energy peaks are reported. [c] Split peak in absorbance.

orientation on the photophysics of the bichromophoric pair. It also allows for a comparison of the relative excited-state energies of the through-space delocalized state with the energies of increasingly conjugated, and hence more stable, chromophores.

Figure 4 contains the absorbance and emission data of **2a**, **2b**, and 4-(2,5-dimethylstyryl)-4′-*tert*-butylstilbene (**2c**). Unless



**2c**
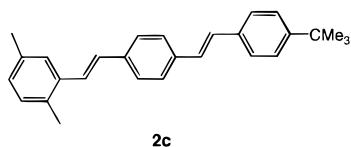
otherwise stated all measurements were made using spectral-grade hexane as solvent. The absorbance and emission spectra of **2c** are characteristic of the distyrylbenzene chromophore which is representative of a small oligomeric unit from a PPV chain. A red-shift of ∼15 nm is observed in the absorbance of the "dimers" **2a** and **2b** relative to **2c** but overall there is little difference in these spectra. The emission frequencies of **2a** and **2b** are indistinguishable and their 16-nm red-shift, relative to the emission of **2c**, can be accounted for by the inherent deformations brought about by the ring strain of the paracyclophane core (also note the emission spectrum of **10** in Figure 8). Note also that all the emission data in Figure 4 retain vibronic structure.

Spectra for compound **9** are presented in Figure 5. Relative to **2a** both absorbance and emission are blue-shifted and the emission band is broader but contains a shoulder, suggestive of vibronic structure.

The photooptical properties of **1a** and **1b** are compared with those of 2,5-dimethylstilbene (**1c**) in Figure 6. These spectra



**1c**
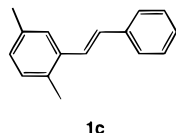
show a red-shift of ∼13 nm for the absorbance spectrum of **1a** relative to **1c**. More pronounced differences are evident in their respective emission spectra ($\lambda_{emis}$(**1a**) = 412 nm vs $\lambda_{emis}$(**1c**) = 355 nm). Whereas **1c** reveals vibronic definition, the broad band shape and larger Stokes shift for **1a** mimics that of excimers.[16] The emission of **1b** is similar to that of **1a**. However, the proximity of the two alkene units in **1b** appears to split the absorbance band ($\lambda_{abs}$ = 264 and 325 nm) relative

to **1c**. The ratio of the two absorption bands for **1b** is found to be independent of temperature. To address the possibility of an equilibriium between two different conformers which give rise to the two absorption bands, we have also carried out variable-temperature $^1$H NMR studies. In these experiments no evidence for a second species was observed to −78 °C, nor did we note significant temperature dependence of the resonances. Furthermore, calculated absorbance spectra using the X-ray coordinates of **1b** match the experimentally measured absorbance spectra (vide infra, Figure 12).

Vibronic structure in the emission of paracyclophane dimers will become highly significant later when the delocalization and energetics of the emitting state are examined and compared. The low-temperature (77 K) emission data in a methyltetrahydrofuran glass for **1a**, **9**, and **2a** are displayed in Figure 7. Note that the vibronic structure becomes better defined with increasing conjugation length. The emission of **1a** is broad and featureless while that of **2a** is sharp. Compound **9** appears to be an intermediate situation.

The spectroscopic data for the monosubstituted derivatives **7** and **10**, shown in Figure 8, closely mimic the trends observed for the symmetric dimers. The emission of **7** is broad and notably red-shifted from the parent dimethylstilbene chromophore while the properties of **10** are similar to those observed for **2c**. Also significant is that **1a** ($\lambda_{emis}$ = 412 nm) emits at longer wavelengths relative to **7** ($\lambda_{emis}$ = 382 nm), suggesting an excited state for **1a** that is diffused to a certain extent over the entire molecule.

Data for the configurational isomers **6a** and **6b** are given in Figure 9. Their absorption spectra differ, as is the case for **1a** and **1b**, implying ground-state electronic effects which are dependent on the relative orientation of the two styrene subunits. For both **6a** and **6b** emission lacks vibronic structure and the emission of **6a** is ∼8 nm red-shifted from that of **6b**. Finally, Figure 10 gives the spectra for the two compounds with the most restricted delocalization, vinylparacyclophane (**5**) and **Pc** itself. Notice the significant red-shift of **5** relative to **Pc**. This observation and the further red-shifts observed for **6a** and **6b** are evidence of stabilization of the emitting species upon substitution of **Pc** with vinyl units.

## Calculational Details

The modeling of chromophore aggregates is simplified when the chromophores are well-separated in space, and their interactions are purely Coulombic (electron exchange is negligible). Each chromophore then retains its own electrons and the system may be described using the Frenkel exciton Hamiltonian.[32,33] This allows the perturbative treatment of intermolecular interactions. The situation is much more complex when electronic states are delocalized among the chromophores. No obvious perturbative theory exists in this case. The calculations of optical excitations are tedious and provide no simple rules for predicting spectroscopic trends.

The collective electronic oscillator (CEO) approach[10−13] provides a new effective computational scheme for electronic excitations of large molecules. The input to the calculation is the reduced single-electron density matrix,[34,35] $\bar{\rho}_{mn} \equiv \langle g|$

(32) Pope, M.; Swenberg, C. E. *Electronic Processes in Organic Crystals*; Claredon Press: New York, 1982.

(33) Silinsh, E. A.; Cápek, V. *Organic Molecular Crystals*; AIP Press, American Institute of Physics: New York, 1994.

(34) McWeeny, R.; Sutcliff, B. T. *Methods of Molecular Quantum Mechancis*; Academic Press: New York, 1976.

(35) Davidson, E. R. *Reduced Density Matrices in Quantum Chemistry*; Academic Press: New York, 1976.
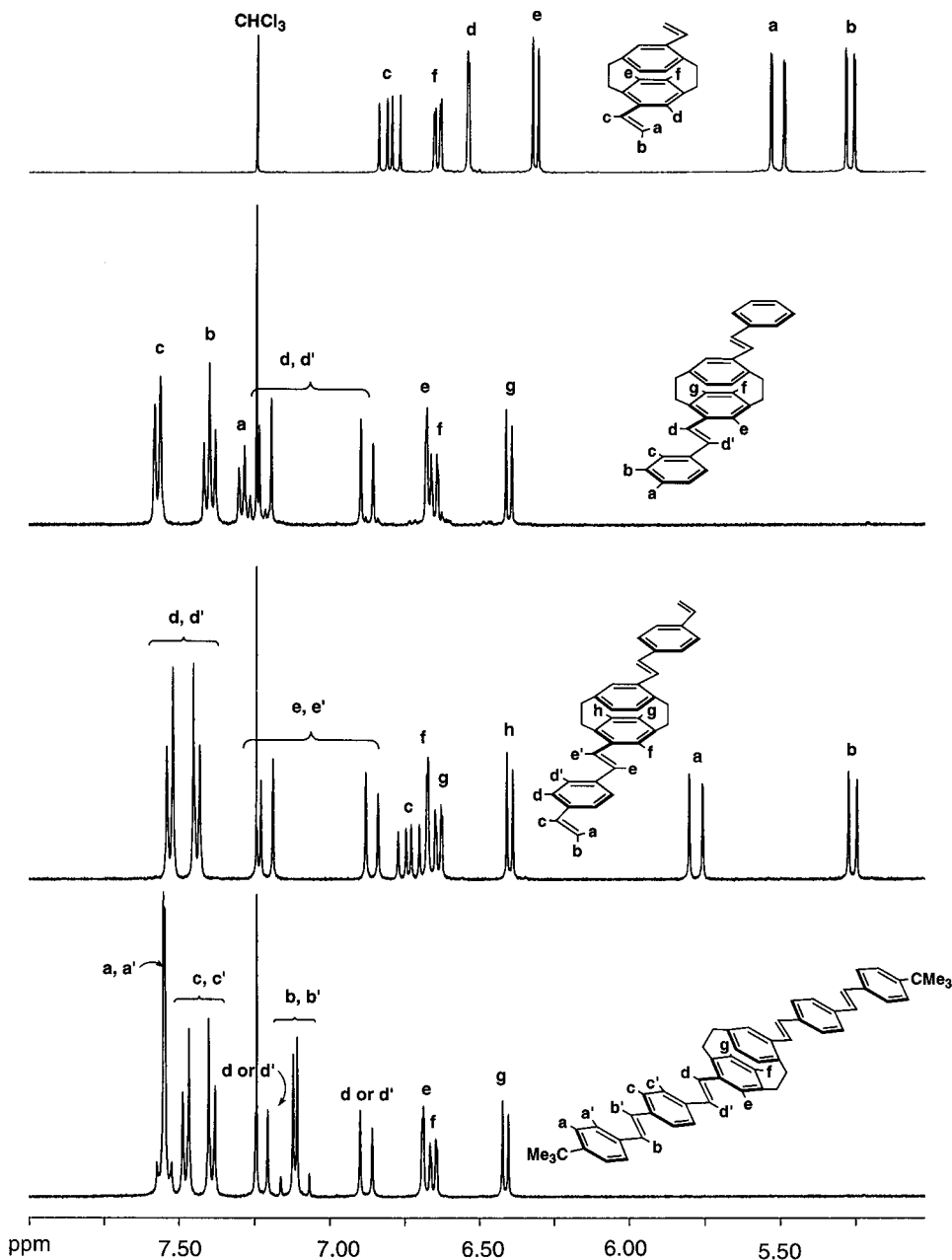
*Stilbenoid Dimers*

*J. Am. Chem. Soc., Vol. 120, No. 36, 1998* 9193



**Figure 3.** ¹H NMR spectra in the aromatic and olefinic region for (a) **6a**; (b) **1a**; (c) **10**, and (d) **2a**.



**Figure 4.** Absorption and emission data for compounds **2a**, **2b**, and **2c**. Emission spectra were measured by exciting at the absorption maxima.



**Figure 5.** Absorption and emission data for compound **9**. The emission spectrum was measured by exciting at the absorption maxima.

$c_m^+ c_n |g\rangle$ where $c_m^+$ ($c_m$) are creation (annihilation) operators of an electron at the *m*-th atomic orbital, and $|g\rangle$ is the ground-state many-electron wave function. The diagonal elements $\bar{\rho}_{nn}$

represent the electronic charge density at the *n*-th orbital, whereas the off-diagonal elements, $m \neq n$, reveal the bonding structure (i.e., bond orders) associated with each pair of atomic
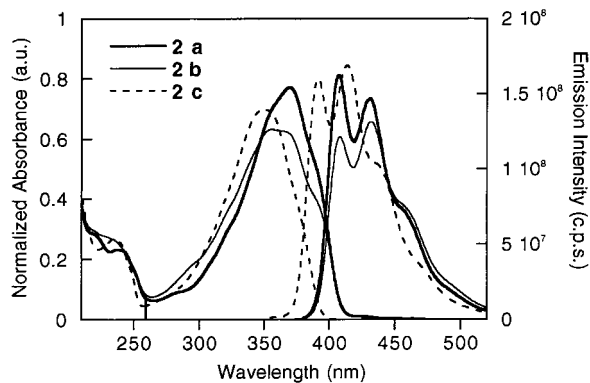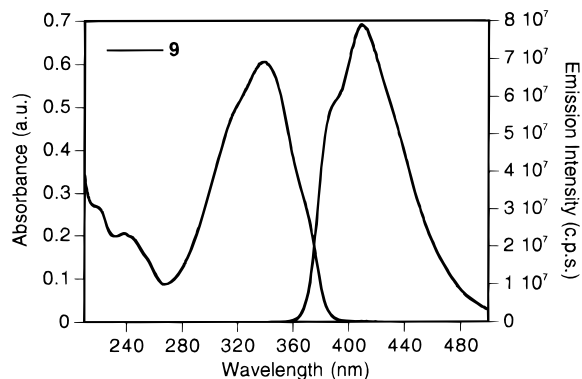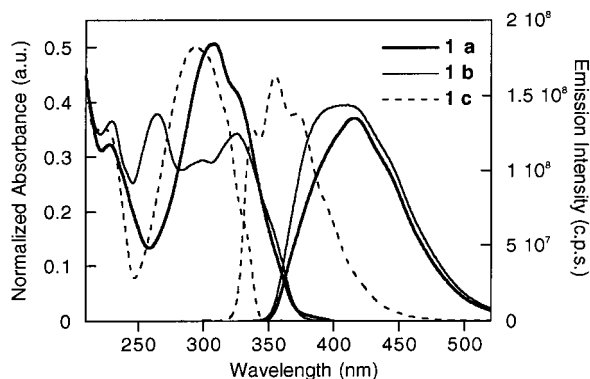
**Figure 6.** Absorption and emission data for compounds **1a**, **1b**, and **1c**. Emission spectra were measured by exciting at the absorption maxima.
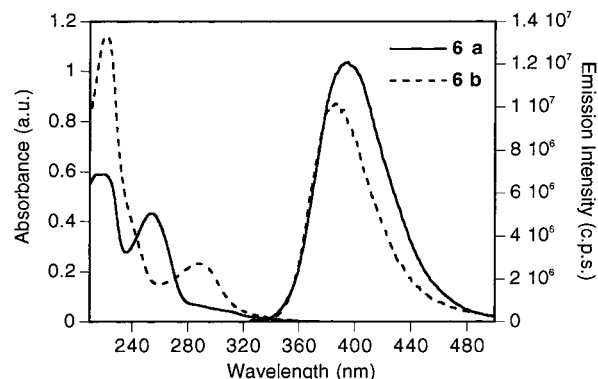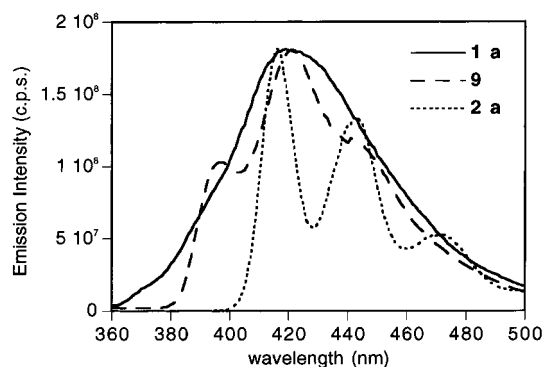


**Figure 7.** Low-temperature emission data (77 K in methyltetrahydrofuran) for compounds **1a**, **9**, and **2a**. Emission spectra were measured by exciting at the absorption maxima.
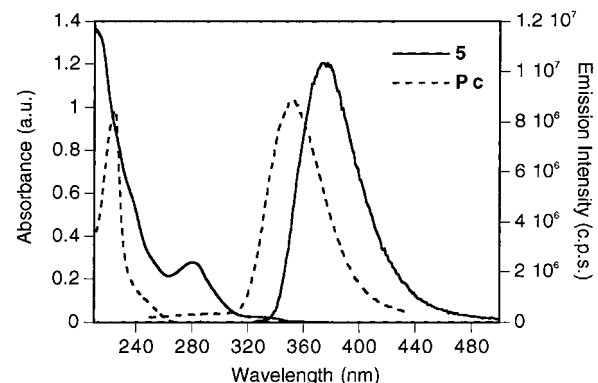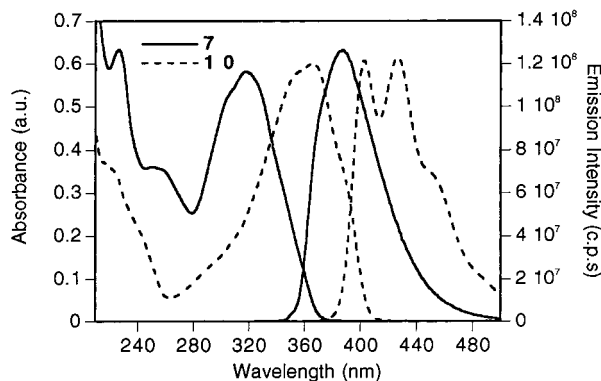


**Figure 8.** Absorption and emission data for compounds **7** and **10**. Emission spectra were measured by exciting at the absorption maxima.

orbitals.[36-39] When the molecule interacts with an external driving field, its electronic density matrix acquires a time-dependent component $\delta\rho(t)$ which can be expanded as

$$\delta\rho(t) = \sum_v a_v(t)\xi_v + a^*_v(t)\xi_v^+ \tag{7}$$

$a_v(t)$ are time-dependent expansion coefficients and the *electronic normal modes* $\xi_v$ represent the optical transitions between

(36) Szabo, A.; Ostlund, N. S. *Modern Quantum Chemistry: Introduction to Advanced Electronic Structure Theory*; McGraw-Hill: New York, 1989.

(37) Mulliken, R. S. *J. Chem. Phys.* **1995**, *23*, 1833; 1841; 2338; 2343.

(38) (a) Reed, A. E.; Curtiss, L. A.; Weinhold, F. *Chem. Rev.* **1988**, *88*, 899. (b) Reed, A. E.; Weinstock, R. B.; Weinhold, F. *J. Chem. Phys.* **1985**, *83*, 735.

(39) (a) Lowdin, P. O. *Phys. Rev.* **1955**, *97*, 1474. (b) Lowdin, P. O. *Adv. Phys.* **1956**, *5*, 1.



**Figure 9.** Absorption and emission data for compounds **6a** and **6b**. Emission spectra were measured by exciting at the absorption maxima.



**Figure 10.** Absorption and emission data for compound **5** and **Pc**. Emission spectra were measured by exciting at the absorption maxima.

the ground state $|g\rangle$ and an electronically excited state $|v\rangle$. Their matrix elements are given by

$$(\xi_v)_{mn} = \langle v|c_m^+ c_n|g\rangle \tag{8}$$

The electronic modes describe collective motions of electrons and holes and carry substantially less information than the many-electron eigenstates but more than required for calculating molecular polarizabilities and spectroscopic observables. The diagonal elements $(\xi_v)_{nn}$ represent the net charge induced on the *n*-th atomic orbital by an external field, whereas $(\xi_v)_{mn}$ *m* $\neq$ *n* is the dynamical bond order representing the joint amplitude of finding an electron on orbital *m* and a hole on orbital *n*. Even though eq 8 involves matrix elements of the global many-electron eigenstates $|v\rangle$ and $|g\rangle$, the CEO can be obtained as eigenmodes of the linearized time-dependent Hartree−Fock (TDHF) equations of motion for the time-dependent density matrix driven by the external field, totally bypassing the calculation of many-electron eigenstates. The eigenfrequencies $\Omega_v$ of these equations provide the optical transition frequencies.[10-13] The frequency-dependent linear polarizability $\alpha(\omega)$ is represented in the form

$$\alpha(\omega) = \sum_v \frac{f_v}{\Omega_v^2 - (\omega + i\Gamma)^2} \tag{9}$$

where $f_v = 2\Omega_v[\mathrm{Tr}(\mu\xi_v)]^2$ is the oscillator strength of the *g* to *v* transition, $\Gamma$ is the line width, and $\mu$ is the dipole moment operator.

Normal modes are commonly used in the description of molecular vibrations. They are collective coordinates which represent coherent motions of the various atoms. Similarly, the
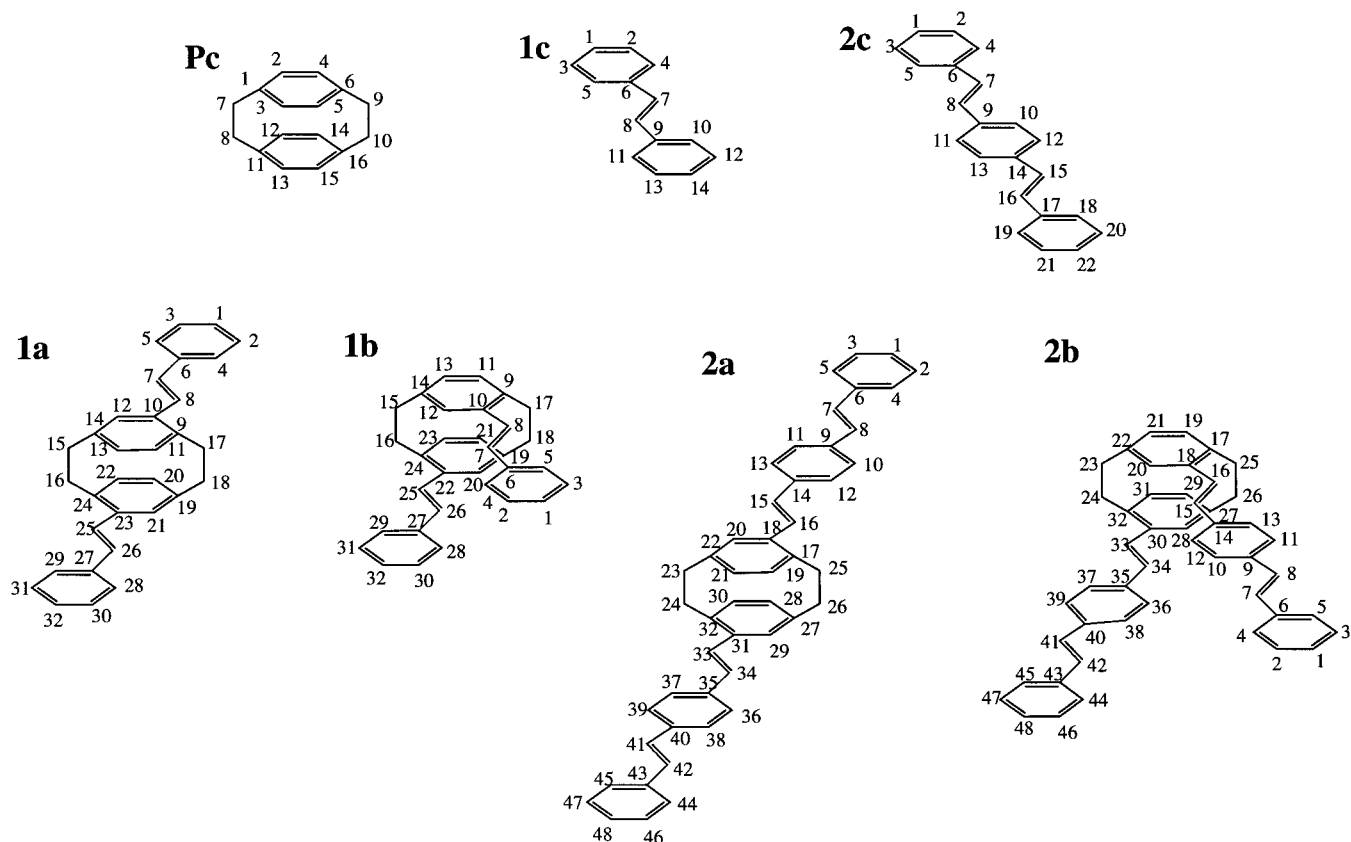
**Figure 11.** Structures and atom labeling of **Pc**, stilbenoid monomers (**1c**, **2c**), and dimers (**1a**, **2a**, **1b**, **2b**).

CEO approach allows us to interpret and visualize electronic motions in terms of collective motions of the electronic density matrix. To compute the electronic modes we further developed the density-matrix-spectral-moments algorithm (DSMA)[12,13] which is a numerically efficient scheme for solving the TDHF equations. The procedure involves computing the set of effective electronic modes which provide the best approximation for the spectrum with a given number of modes. Making use of the Lanczos algorithm, it allows us to focus solely on the main oscillators which contribute to the optical response. The DSMA makes it possible to compute optical spectra even for very large molecules with hundreds of heavy atoms.[12,13]

The CEO approach has been applied previously to explain the response of naphthalene dimers and trimers[40] in terms of monomer response functions. These studies used the simple Pariser−Parr−Pople Hamiltonian. The present work uses the higher level INDO/S Hamiltonian, a different, more compact definition of the CEO (based on the electron−hole part of the density matrix) and the improved DSMA.[12,13]

**Electronic Modes of the Monomeric Building Blocks.** The molecules studied along with their atomic labeling are displayed in Figure 11. We considered the dimer structures **1a**, **1b**, **2a**, **2b**, the monomer units **1c**, **2c**, as well as **Pc**, which is the central piece of all dimers studied. Ground-state geometries were obtained using the crystal X-ray diffraction data given in ref 19.[41] The ZINDO code was utilized to generate INDO/S[42,43]

(40) Wagersreiter, T.; Mukamel, S. *J. Chem. Phys.* **1996**, *105*, 7995.

(41) The geometries were experimentally measured for molecules **1a** and **1b**; the geometries of **Pc** and **1c** were extracted from **1a** X-ray data; the geometries of **2a**, **2b**, and **2c** were assembled from **1a** and **1b** X-ray data by elongating the stilbene units.

(42) Stavrev, K. K.; Zerner, M. C.; Meyer, T. J. *J. Am. Chem. Soc.* **1995**, *117*, 8684.

(43) Broo, A.; Zerner, M. C. *Chem. Phys.* **1995**, *196*, 407; **1995**, *196*, 423.

Hamiltonian and the CEO/DSMA procedure was then applied to compute the linear absorption spectra. In all calculations we used the empirical line width $\Gamma = 0.2$ eV, and satisfactory convergence of the linear absorption was achieved using 10−15 effective electronic modes.

The calculated spectra of the monomers **1c** and **2c** are displayed in Figure 12 (solid lines). Experimental absorption and fluorescence spectra are shown by dashed and dotted lines, respectively. We denoted the lowest strong absorption peak of **1c** and **2c** as II. (The reason for this notation will become clear in the next section where we consider the dimer spectra.) No geometry optimization was carried out and no parameters were tuned or rescaled. Nevertheless the theoretical spectra are in excellent agreement with experiment.[44]

To explore the origin of the various peaks we examined the collective modes corresponding to these electronic excitations. By displaying the matrices $\xi_v$ using two-dimensional plots, we establish a direct real-space connection between the optical response and the dynamics of charges upon optical excitation. The size of the matrix is equal to the number of carbon atoms in the molecule, labeled according to Figure 11; the ordinate and abscissa represent an electron and a hole, respectively.

Panel **1c**($\rho$) in Figure 13 displays the ground-state density matrix $\bar{\rho}$ of **1c**. The density matrix is dominated by the diagonal and near-diagonal elements, reflecting the bonds between nearest neighbors. The aromatic rings (corners of the matrix) and the vinylic double bond (center of the matrix) are clearly identified. **1c**(II) shows the electronic mode of peak II in **1c**. This mode is completely delocalized over the entire molecule with the strongest coherences (off-diagonal elements) in the double bond

(44) In the Experimental Section measurements **1c** and **2c** are substituted at positions 2 and 5 by methyl groups; **2c** is substituted at position 22 by *tert*-butyl group; **2a** and **2b** are substituted at 1 and 48 by *tert*-butyl groups.
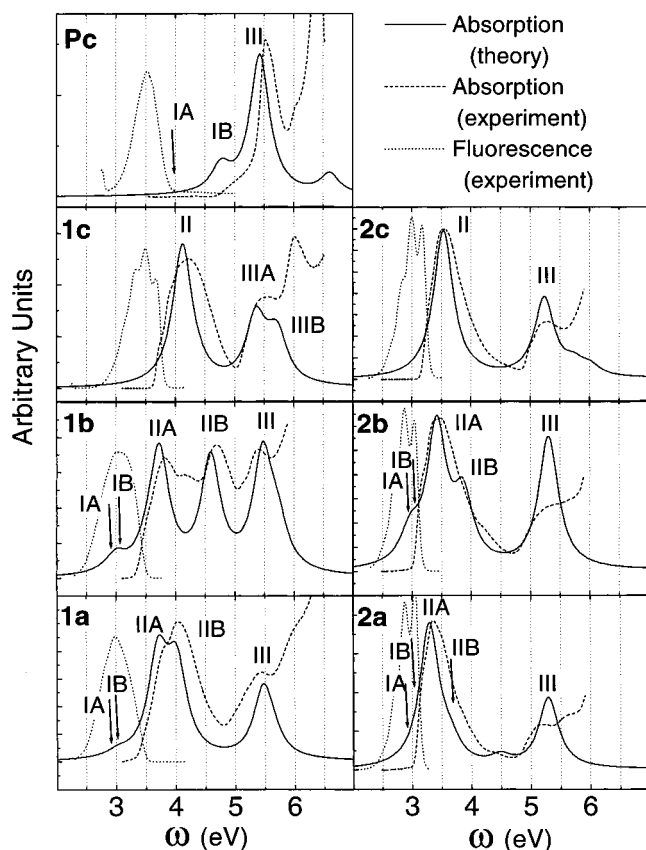
9196  *J. Am. Chem. Soc., Vol. 120, No. 36, 1998*

*Bazan et al.*



**Figure 12.** Calculated (solid lines) and experimental (dashed lines) absorption spectra and experimental (dotted lines) fluorescence spectra of the molecules presented in Figure 11.

of the vinylic group. The following two modes of stilbene (**1c**(IIIA) and **1c**(IIIB)) are localized on the first and the second arene rings, respectively.

The second column in Figure 13 shows the dominant electronic modes of **2c**. They have basically the same properties as the corresponding modes of the shorter molecule **1c**. The delocalized mode II is significantly red-shifted. Our calculations lumped all localized transitions III to a single effective mode localized at the phenyls.

Before turning to the dimer spectra we shall examine the calculated absorption spectrum of **Pc** which in an important common unit of all dimers studied. The electronic properties of **Pc** have been extensively studied.[45,46] The calculated and experimental spectra of **Pc** are displayed in the top panel in Figure 12. We consider three electronic excitations. The lowest transition IA with frequency $\Omega_{IA} = 3.95$ eV is forbidden in linear absorption and compare well with experiment (4.1 eV).[47] IB is the first peak in absorption ($\Omega_{IB} = 4.77$ eV) with a weak dipole along the benzene long axis. Peak III ($\Omega_{III} = 5.5$ eV) dominates the absorption. Our calculated frequencies compare well with experiment (4.06, 5.12, and 5.42 eV).[46] **Pc**($\rho$) shown in Figure 13 represents the ground-state density matrix $\bar{\rho}$ of **Pc**. The aromatic rings at the corners and two bridge shoulders in the center are clearly identified. **Pc**(IA) shows the lowest electronic modes in **Pc**. The excitation is localized on the aromatic rings and shows the strong electronic coherence (which

is a signature of charge delocalization) between them. **Pc**(IB) is also delocalized over the entire molecule but with a weaker coherence between aromatic rings than **Pc**(IA). In contrast, the **Pc**(III) mode shows very small charge delocalization between arene rings. Modes IA and IB are delocalized and are therefore red-shifted compared to mode III which is localized on the arene rings. Due to its localized nature, mode III has roughly the same structure and transition frequency (5.3−5.4 eV) for all three molecules **Pc**, **1c**, and **2c**.

**Electronic Modes of Dimers.** Panel **1a**($\rho$) in Figure 13 displays the ground-state density matrix $\bar{\rho}$ of **1a**. The plot shows that dimerization hardly affects the ground state. The density matrices of the **Pc**($\rho$) and **1c**($\rho$) units can be easily identified in the density matrices of **1a**. The ground-state density matrices of other dimers (not shown) behave similarly.

We next turn to the optical excitations of the dimers. Panel **1a**(IA) of Figure 14 shows the lowest frequency electronic mode IA of **1a**. This mode is virtually the same as **Pc**(IA). It is essentially localized on the paracyclophane, has a vanishing oscillator strength, and represents the charge delocalization between monomers. The following mode **1a**(IB) corresponds to **Pc**(IB) and similarly has a weak oscillator strength. However, the small delocalization to neighboring vinylic groups leads to dramatic red-shift in frequency from 3.95 to 2.91 eV for IA and from 4.77 to 3.04 eV for IB.

Mode **1a**(IIA) resembles mode II of the monomer **1c** (diagonal blocks), but shows some electronic coherences between chromophores (off-diagonal blocks). The structure of **1a**(IIB) is similar to **1a**(IIA) but it shows a slightly different distribution of coherences and stronger charge delocalization between monomers. The coupling of the monomeric modes **1c**(II) leads to a Davydov-like splitting resulting in modes IIA and IIB in the dimers.[48] The frequency splitting reflects the interaction strength between monomers. The high-frequency mode **1a**(III) is localized mostly on the aromatic rings at the edge, and weakly penetrates to the central **Pc** unit, with a small trace of optical coherences between the monomers. This mode shows about the same localization properties as **1c**(II). We thus conclude that the electronic excitations of the dimer **1a** can be constructed from the excitations of its **Pc** and **1c** units, perturbed by interaction between monomers.

We next compare electronic modes of different dimers to investigate how geometry and monomer size affect charge delocalization. The second column in Figure 14 shows the electronic modes of **1b** (for atom labeling see Figure 12). The dominant optical excitations of the larger dimers **2a** and **2b** are displayed in the third and fourth columns.

The lowest frequency modes IA and IB and the high-frequency mode III are localized and hardly change upon dimerization. Modes IA with frequency 2.9 eV and mode IB with frequency 3 eV originating from **Pc**(IA) and **Pc**(IB), respectively, are virtually the same for all four dimers. Mode III which can be attributed to **1c**(III) and **2c**(III) is localized on the arene rings and shows a weak charge delocalization between monomers for all four molecules. However, it has a quite different diagonal distribution of optical coherences for short (**1a**, **1b**) and long (**2a**, **2b**) dimers. The localized nature of mode III explains the invariance of its transition frequency (5.3−5.5 eV).

(45) Canuto, S.; Zerner, M. C. *J. Am. Chem. Soc.* **1990**, *112*, 2114.

(46) Iwata, S.; Fuke, K.; Sasaki, M.; Nagakura, S.; Otsubo, T.; Misumi, S. *J. Mol. Spectrosc.* **1973**, *46*, 1.

(47) Experimentally this transition is weakly vibronically allowed by borrowing intensity from IB (ref 45). It can be seen by plotting the experimental absorption in logarithmic scale. The fluorescence of **Pc** originates primarily from IA (ref 45).

(48) The term "Davydov splitting" usually refers to the splitting of degenerate states in molecular aggregates and crystals in which intermolecular interactions are electrostatic, and are described by the Frenkel exciton Hamiltonian. In contrast, the coupling between electronic modes in dimers includes electrostatic as well as exchange interactions, which result in interchromophore electronic coherence. These may not be described by Frenkel exciton Hamiltonian.
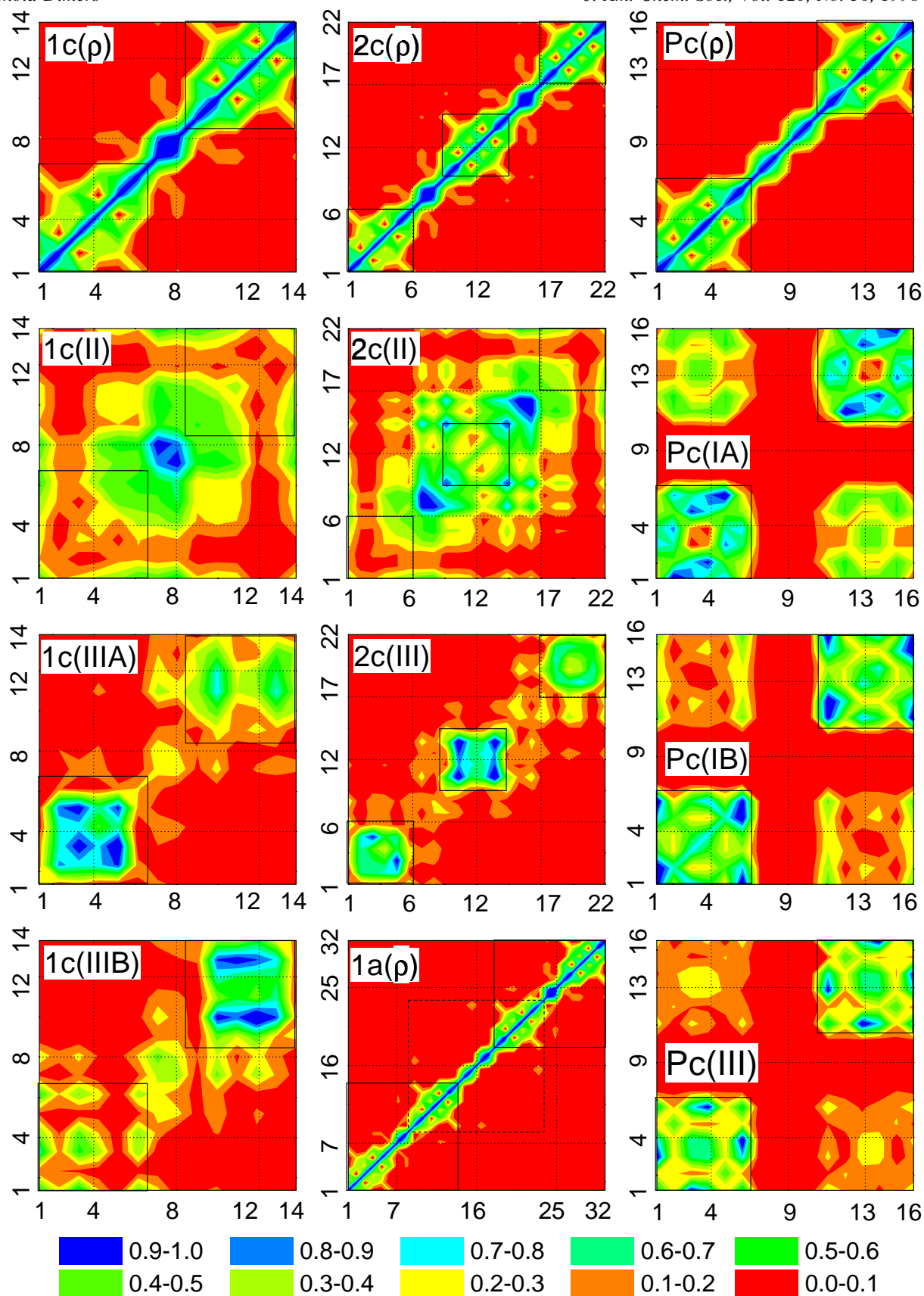
**Figure 13.** Contour plots of ground-state density matrices and the electronic modes which dominate the optical absorption of monomers **1c** and **2c**. The axis labels represent the individual carbon atoms as labeled in Figure 11. The panels indicate the molecule (Figure 11) and the electronic mode (Figure 12) (e.g., **1c**($\rho$) is the ground-state density matrix of molecule **1c**; **Pc**(III) is mode III of **Pc**. The aromatic ring units are shown by solid rectangles. The color code is given in the bottom row. Mode frequencies of **1c** ($\Omega_{II} = 4.12$ eV, $\Omega_{IIIA} = 5.36$ eV, $\Omega_{IIIB} = 5.73$ eV); **2c** ($\Omega_{II} = 3.53$ eV, $\Omega_{III} = 5.25$ eV); **Pc**($\Omega_{IA} = 3.95$ eV, $\Omega_{IB} = 4.77$ eV, $\Omega_{III} = 5.5$ eV).

**Table 2.**   Experimentally Determined Quantum Yields

| compound | $\Phi_{PL}$ (%) |
| --- | --- |
| **1a** | 30 |
| **2a** | 56 |
| **2c** | 62 |

**Table 3.**   Double Exponential Fits to the Fluorescence Decay after Deconvolution from the Instrument Impulse Response[a]

| compound | $\tau_1$ | $B_1$ | $\tau_2$ | $B_2$ |
| --- | --- | --- | --- | --- |
| **1a** | 5.2 | 71 | 2.0 | 29 |
| **2a** | 1.2 | 100 | | |
| **2c** | 1.1 | 100 | | |

[a] The time dependence of the fluorescence intensity [$I_f(t)$] was modeled using the equation $I_f(t) = B_1 \exp(-t/\tau_1) + B_2 \exp(-t/\tau_2)$ where $\tau_1$ and $\tau_2$ denote lifetimes and $B_1$ and $B_2$ are the amplitude coefficients. On the basis of multiple measurements the relative error on the values of $\tau$ and $B$ was approximately ±5%.

The bulk (delocalized) mode II appearing in the spectra as peaks IIA and IIB changes significantly upon dimerization and shows charge delocalization which depends on the molecule. Comparison of IIA and IIB leads to the following observations: (i) charge delocalization is much stronger for molecules with *ortho* (**1b** and **2b**) than with *para* (**1a** and **2a**) orientation because the vinylic groups where the monomer bulk mode II is concentrated in **2b** are geometrically closer with separation of about 4 Å and strongly interact with each other; (ii) charge delocalization is stronger for the shorter molecules (**1a** and **1b**) compared with **2a** and **2b** because in the former the electron–hole pair "spends more time" on the **Pc** unit which promotes charge delocalization; (iii) the stronger the charge delocalization between monomers, the less IIA and IIB resemble the original **1c**(II) and **2c**(II) modes. The splitting depends on the optical coherences between monomers in the mode. For example, **1b** exhibits the strongest coherences in mode II and shows the largest splitting ∼0.9 eV between IIA and IIB peaks. **2a** has the weakest coherences in mode II, showing a much smaller splitting ∼0.3 eV. IIA is much stronger in absorption compared to IIB, which leads to a single peak spectrum of type II.

**Fluorescence Lifetimes Stokes Shifts and Quantum Yields.** Emission quantum yields ($\Phi_{PL}$) and fluorescence decay measurements provide information complementary to the steady-state data and give insight into the dynamic processes of the excited state. In this section we compare the lifetime decay properties of compounds **1a** and **2a** with those of the "parent" chromophores **1c** and **2c**. The electronic description of the monomers and dimers, given above, should be consistent with these measurements.

Table 2 contains experimentally determined $\Phi_{PL}$ values for **1a** and **2a,c** under identical conditions. Exact details for these determinations are found in the Experimental Section, and we estimate the error in these values to be approximately ±5%. For the fluorescence decay measurements we relied on the technique of time correlated single photon counting on a nanosecond time scale.[49,50] Figure 15 shows that the fluorescence lifetime of **1a** is approximately 10-fold greater than that of **1c**. The measured decay profiles were fitted using monoexponential and biexponential functions and some of the resulting parameters are shown in Table 3. As shown in Figure 16, there is virtually no difference in the fluorescence decay dynamics

of **2a** and **2c**. Both show nearly monoexponential decays with a lifetime of ∼1.1–1.3 ns (Table 3). Note that this value is similar to that measured for the copolymer PPV$_{10}$-*block*-polyNBE$_{200}$ in dilute solution.[51]

To study the fluorescence dynamics we calculated the experimental radiative decay rates of **1a**, **2a**, and **2c** using $\gamma^r = \Phi_{PL}/\tau$, where the values for $\Phi_{PL}$ and the fluorescence lifetime $\tau$ are given in Tables 2 and 3, respectively. The radiative decay rate of **1c** was reported in ref 53. We also calculated the theoretical radiative decay rate $\gamma_v^r$ of **1a−c** and **2a−c** using the expression:[52]

$$\gamma_v^r = {}^2\!/_3 f_v \Omega_v^2$$

Here $f_v$ and $\Omega_v$ are the oscillator strength and the frequency of mode $\nu$ (see eq 9).

Assuming that only the delocalized mode IIA participates in the fluorescence of long molecules, we obtain 0.7 and 0.67 ns$^{-1}$ for the monomer (**2c**) and the dimer (**2a**) decay rates. These compare well with experimental values of 0.55 and 0.5 ns$^{-1}$, respectively. The calculated rate constant is somewhat larger because molecular vibrations and solvent effects which reduce electronic coherence were not taken into account. The calculated radiative lifetime of stilbene **1c** (0.52 ns$^{-1}$) is consistent with the experimental value 0.62−0.67 ns$^{-1}$.[53] The radiative rates of the short dimers behave markedly different. The experimental radiative rate of **1a** is significantly slower and the quantum yield is lower than **2a**. Assuming that only the localized mode IA participates in fluorescence of the short dimer **1a**, we obtained 0.05 ns$^{-1}$ for the radiative rate compared with the experimental value of 0.06 ns$^{-1}$. The calculated rate is underestimated because the fluorescence depends also on states IB and possibly IIA of **1a**. Thus the weak oscillator strengths of IA and IB in the short dimers, **1a** and **1b**, and the fast relaxation to these states lead to the longer fluorescence lifetime.

The qualitative trends of the experimental fluorescence spectra displayed in Figure 12 (dotted curves) can be understood by examining the computed electronic modes. Fluorescence spectra of the monomers, **1c** and **2c**, both show distinct vibronic structure and have similar Stokes shifts of 0.7 and 0.5 eV, respectively (defined as the shift between the strongest peaks in absorption and emission). The fluorescence spectra of dimers **2a** and **2b** have virtually identical shapes to the monomer **2c** (see Figure 4) and show Stokes shifts 0.4, 0.5, and 0.5 eV, respectively. The spectra of dimers, **1a** and **1b**, are markedly different. They are broad and featureless, show no vibronic structures, and their shapes resemble the fluorescence of **Pc** (see Figure 6). They show nearly no shift relative to **10**, the monomer containing the **Pc** moiety. The Stokes shifts of **1a** and **1b** are large compared to **1c** (0.8, 0.9, and 0.7 eV, respectively but not compared to **7**. These observations can be explained by assuming that in the short dimers **1a** and **1b** the optically excited IIA state relaxes to the lower lying IA and IB states. The fluorescence originates from states IA and IB which are red-shifted by 0.93 and 0.8 eV with respect to IIA. This suggests that the large Stokes shift may be electronic in origin. However, in the absence of additional information of excited-state geometries, nuclear contribution to the Stokes shift cannot be completely ruled out.

(49) Lakowicz, J. R. *Principles of Fluorescence Spectroscopy*; Plenum: New York, 1983.

(50) A detailed fluorescence decay analysis for a family of paracyclophane structures will be the basis of a future publication. Heinrich, J.; Atherton, S.; Bazan, G. C. Unpublished work.

(51) Bazan, G. C.; Miao, Y.-J.; Renak, M. L.; Sun, B. J. *J. Am. Chem. Soc.* **1996**, *118*, 2618.

(52) Mukamel, S. *Principles of Nonlinear Optical Spectroscopy*; Oxford Press: New York, 1995.

(53) Greene, B. I.; Hochstrasser, R. M.; Weisman, R. B. *Chem. Phys.* **1980**, *48*, 289.
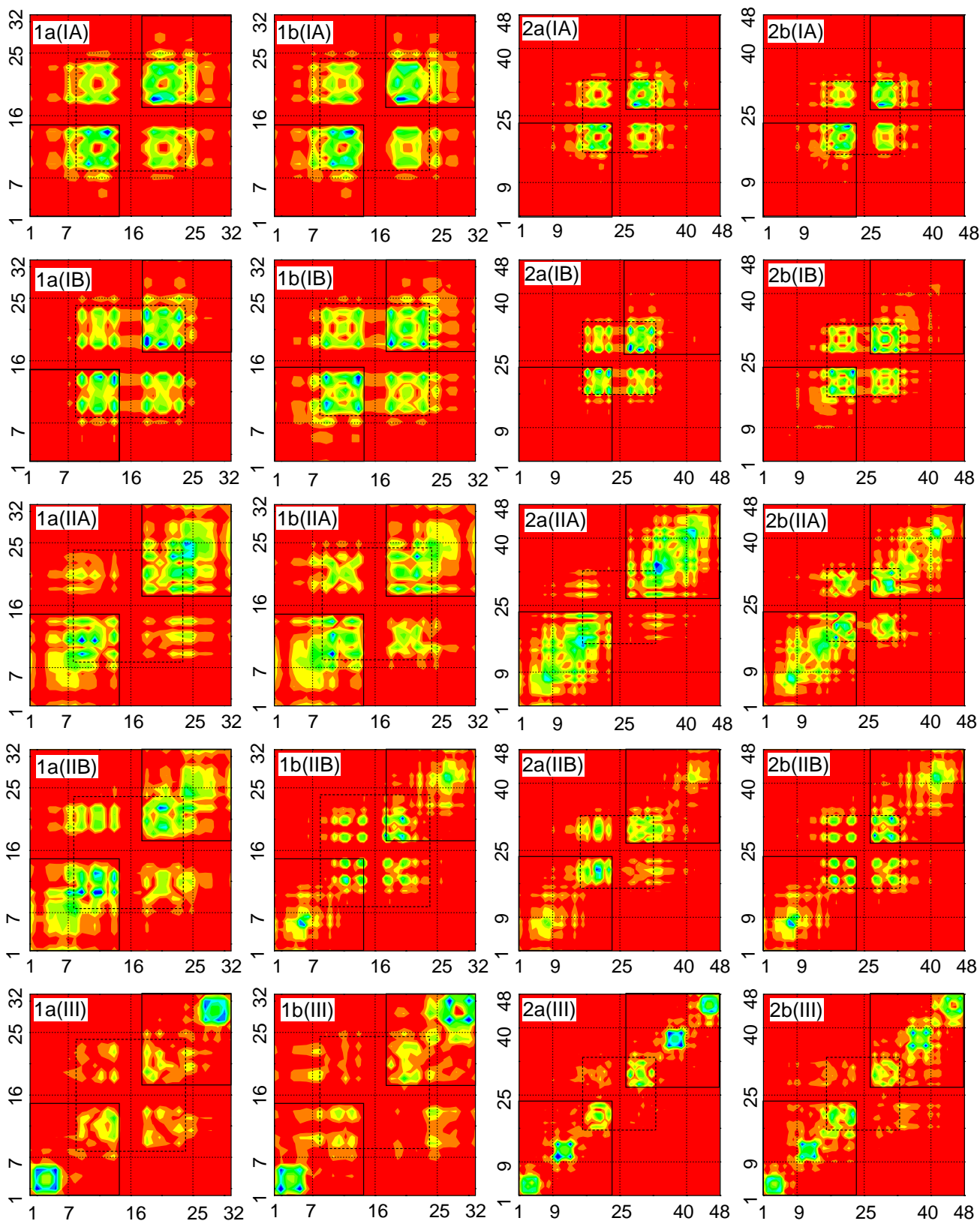
**Figure 14.** Contour plots of electronic modes which dominate the absorption dimers. The axis labels represent the individual carbon atoms as labeled in Figure 11. The panels indicate the molecule (Figure 11) and the electronic mode (Figure 12). The monomers **1c** and **2c** units are shown by solid rectangles. The paracyclophane **Pc** unit is shown by dashed rectangle. The color code is given in Figure 13. Mode frequencies of **1a** ($\Omega_{IA}$ = 2.91 eV, $\Omega_{IB}$ = 3.03 eV, $\Omega_{IIA}$ = 3.69 eV, $\Omega_{IIB}$ = 4.02 eV, $\Omega_{III}$ = 5.46 eV); **1b** ($\Omega_{IA}$ = 2.92 eV, $\Omega_{IB}$ = 3.01 eV, $\Omega_{IIA}$ − 3.72 eV, $\Omega_{IIB}$ = 4.59 eV, $\Omega_{III}$ = 5.47 eV); **2a** ($\Omega_{IA}$ = 2.91 eV, $\Omega_{IB}$ = 3.03 eV, $\Omega_{IIA}$ = 3.29 eV, $\Omega_{IIB}$ = 3.61 eV, $\Omega_{III}$ = 5.29 eV); **2b** ($\Omega_{IA}$ = 2.92 eV, $\Omega_{IB}$ = 3.01 eV, $\Omega_{IIA}$ = 3.41 eV, $\Omega_{IIB}$ = 3.86 eV, $\Omega_{III}$ = 5.30 eV).

In contrast, in longer dimers **2a** and **2b**, the state IIA is significantly red-shifted since it is delocalized, whereas the states IA and IB do not shift significantly. Semiempirical calculations tend to underestimate the energies of the low-lying states in
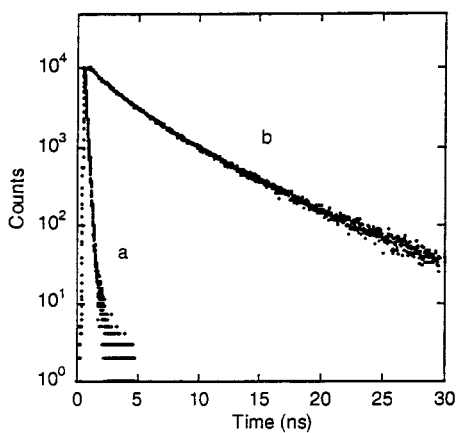
**Figure 15.** Fluorescence lifetime measurements of compounds **1c** (a) and **1a** (b).
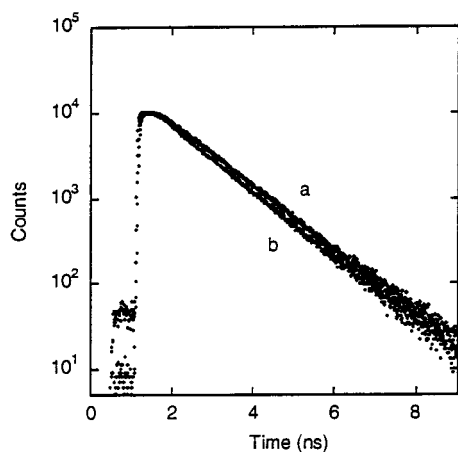


**Figure 16.** Fluorescence lifetime measurements of compounds **2a** (a) and **2c** (b).

cyclophanes.[45] For example, our calculations give the energy of IA in **Pc** 0.15 eV lower than the experimental value. Therefore, we conclude that within the accuracy of semiempirical calculations the energies of states IA and IIB are comparable with energy of the optically active transition spectra IIA in **2a** and **2b**. Consequently the separation between II and IA(IB) in long dimers is only about 0.33 eV (0.2 eV). Infact, the states IA and IB lie within the line width of optically active transition IIA. Consequently, the relaxation of population to states IA and IB upon excitation of state IIA is less important and the emission originates primarily from the initially excited state.

**Summary Discussion and Conclusion**

We have demonstrated that it is possible to synthesize a sequence of cyclophane structures that hold together chromophores of increasing conjugation length. Heck-type reactions of the brominated cyclophanes **3** and **4a,b**, as shown by eqs 1−6, have been found to be the most reliable entry into phenylenevinylene structures. It should be mentioned that the iodocyclophane counterparts work better in this respect[54] but are more difficult to prepare in large quantities. The availability of pseudo-*para* and pseudo-*ortho* isomers **4a** and **4b** allows for the investigation of orientational effects.

Important insight into the photophysics of bichromophoric phane dimers can be obtained from the optical spectra shown in Figures 3−10. As shown by Figures 6 (for **1a** and **1b**) and
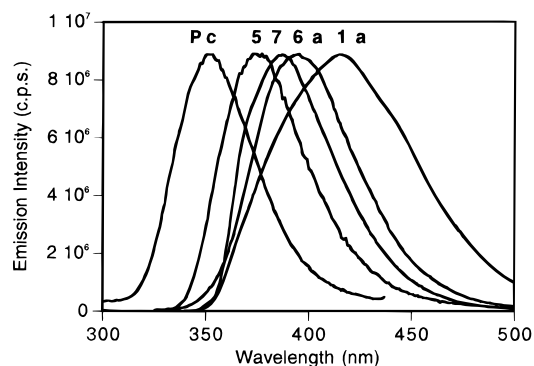


**Figure 17.** Collected emission data for compounds **Pc**, **5**, **7**, **6a**, and **1a**.

9 (for **6a** and **6b**) the absorption data are affected by the relative orientation of the two chromophores when these are either styrene or stilbene. This perturbation is consistent with ground-state interactions between the two subunits. Despite containing the same structural relationship as for **1a** and **1b**, the absorption spectrum of **2a** is nearly identical to that of **2b** (Figure 4).

Exocyclic sustituents make a contribution to the excited-state energy of the "phane" state. This effect is illustrated in Figure 17 where the emission maxima for different derivatives show a progressive red-shift, dependent on the conjugation length and number of substituents linked to **Pc**. Therefore, the "phane" state diffuses partly from the **Pc** core onto the conjugated substituents.

The nature of the optical excitations of **1a,b** and **2a,b** is illustrated by using a two-dimensional representation of electronic normal modes in real space. These plots reveal an off-diagonal size associated with relative (center of mass) motion of electron−hole pairs created upon optical excitation. The lowest frequency electronic mode, localized on the paracyclophane group of the dimer, makes a small contribution in absorption of all aggregates, but dominates the emission spectra of small dimers **1a** and **1b**, leading to a large electronic Stokes shift. The two lower energy electronic modes, localized on the monomeric units, dominate the linear absorption of all aggregates and the fluorescence of long dimers **2a** and **2b**. Their electronic coherences reflect the charge delocalization between monomers and strongly depend on the relative chromophore orientation. These calculations account for all observed trends in absorption spectra, fluorescence Stokes shift, and radiative lifetimes, and establish a rigorous connection between the optical response of aggregates and the properties of the monomers.

The CEO analysis leads to the qualitative energy diagram for the photoexcitation dynamics shown in Scheme 1. We assume that in all cases the most significant absorption is attributed to the "monomer" chromophore, i.e. stilbene in the case of **1a**. There is a second excited state to consider, namely one which contains the paracyclophane core. This state will be referred to as the "phane" state and contains the through-space ($\pi−\pi$) delocalization.[45,46] Emission from this state is broad and featureless and similar to that which characterizes excimers. Two situations may be encountered after photon absorption. For the smaller chromophores styrene and stilbene the energy of the localized excitation is higher than that of the state containing the paracyclophane core (a in Scheme 1). Energy migration[55] transfers the excitation from the localized "monomer" and emission takes place from the "phane" state. In addition, the extinction coefficient for direct excitation from

(54) Miao, Y.-J, Ph.D. Thesis, University of Rochester, 1997.

(55) Here we use the term "energy migration" but it could be argued that the term "internal conversion" is adequate as well.

**Scheme 1**



**a**, for R = H, Ph　　　　　　　**b**, for R* = H,4-$^t$Bu- Ph
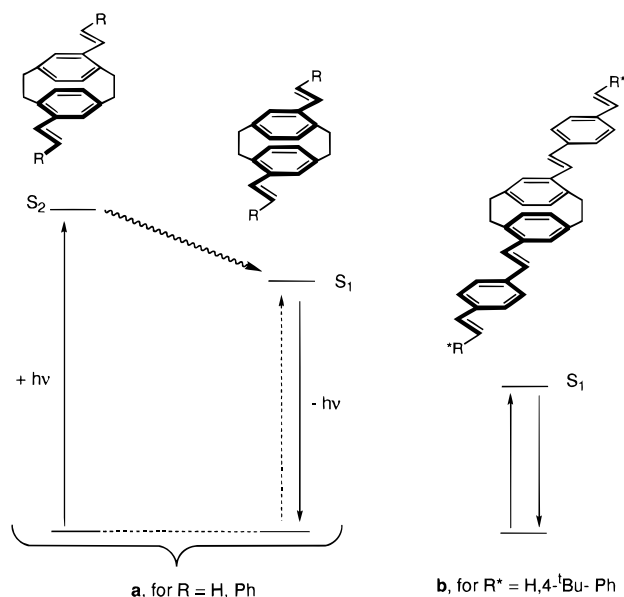
the ground state is weak. Population of the "phane" state via energy transfer should result in a relatively long-lived excited state, as observed in Figure 15.

The second situation is when the energy of the "monomer" is lower than the corresponding "phane" state (b in Scheme 1). This is the situation for vinylstilbene (i.e., **9**) and distyrylbenzene (i.e., **10** or **2a,b**). Under these circumstances there is no driving force for energy migration and the excitation remains localized. Except for the shift due to the **Pc** moiety (see **10** in Figure 8), there is therefore negligible difference between the spectra of the parent compound **2c** and the dimers **2a,b**.

## Experimental Section

**General Details.** All manipulations involving air-sensitive organometallic reagents were carried out using techniques as described previously.[56] ^{1}H and ^{13}C{^{1}H} NMR spectra were recorded on a Bruker AMX-400 NMR spectrometer operating at 400.1 and 100.6 MHz, respectively. UV−vis absorption spectra were recorded on a Perkin-Elmer Lambda 19 spectrophotometer and photoluminescence spectra on a Spex Fluorolog 2 spectrometer in spectral grade hexane. High-resolution mass spectrometry was performed by the Nebraska Center for Mass Spectrometry at the University of Nebraska−Lincoln. Elemental analysis were performed by Desert Analytics. Reagents were obtained from Aldrich and used as received. Pseudo-*p*- and pseudo-*o*-dibromo[2.2]paracyclophane were prepared and purified as described previously.[21] Flash chromatographic separations were carried out using the Biotage Flash 40 system.

Solutions for fluorescence measurements were prepared to specific concentrations such that the maximum absorbance was ∼0.1. All manipulations were performed inside a nitrogen-filled glovebox and the solutions were introduced into a quartz cuvette equipped with a Teflon needle valve to minimize contact with oxygen. Fluorescence was measured at right angles using a 1-cm cuvette. The quantum yield is calculated from the relation:

$$\Phi_{unk} = \Phi_{std}\left[\frac{A_{std}(\lambda_{std})}{A_{unk}(\lambda_{unk})}\right]\left[\frac{I_{std}(\lambda_{std})}{I_{unk}(\lambda_{unk})}\right]\left[\frac{D_{unk}}{D_{std}}\right]$$

where the subscripts std and unk indicate the standard and unknown sample, $A(\lambda)$ corresponds to the absorbance of the solution at the exciting wavelength $\lambda$, $I(\lambda)$ is the intensity of the exciting beam

(assumed to be equal for both measurements), and $D$ is the integrated luminescence spectrum. Stilbene and anthracene[57] are used as standards in all quantum yield determination experiments. The details for the lifetime measurements have appeared previously.[58]

**4-Vinyl[2.2]paracyclophane (5).** A high-pressure steel bomb charged with 4-bromoparacyclophane (4.31 g, 15.0 mmol), Pd(OAc)$_2$ (52 mg, 0.23 mmol), tri(*o*-tolyl)phosphine (282 mg, 0.93 mmol), triethylamine (5 mL), and DMF (50 mL) was pressurized with ethylene (100 psi) and vented three times to purge the system of oxygen. The vessel was then pressurized with ethylene (100 psi) and sealed and then heated to 100 °C while stirring with a mechanical stirrer for 2 days. The reaction mixture was then diluted with water to precipitate the crude product, which was filtered off and rinsed with additional water. This material was dissolved in chloroform and filtered into a clean flask to remove insoluble palladium impurities, then dried (MgSO$_4$). Purification by flash chromatography (hexanes) yields 2.9 g (83%) of pure white powder. ^{1}H NMR (CDCl$_3$): 6.78 (dd, $J = 17.4$, 10.9 Hz, 1 H); 6.70 (dd, $J = 7.9$, 1.8 Hz, 1H); 6.53−6.37 (multiplets, 6H); 5.52 (dd, $J = 17.4$, 1.4 Hz, 1 H); 5.27 (dd, $J = 10.9$, 1.4 Hz, 1 H); 3.46 (m, 1 H); 3.11−2.91 (m, 6 H); 2.79 (m, 1 H). Calcd for C$_{18}$H$_{18}$: C, 92.3; H, 7.7. Found: C, 92.02; H, 7.91.

**4,16-Divinyl[2.2]paracyclophane (6a).** A 50-mL round-bottom flask charged with a Teflon-coated stir bar, 4,16-dibromoparacyclophane (366 mg, 1 mmol), Pd(OAc)$_2$ (10.5 mg, 0.047 mmol), tris(*o*-tolyl)-phosphine (71 mg, 0.23 mmol), triethylamine (1 mL), and DMF (5 mL) was placed into a high-pressure steel bomb containing a thin layer (2 cm) of sand. (The sand was used to efficiently transfer heat from the walls of the bomb to the round-bottom flask.) The vessel was then pressurized with ethylene (100 psi) and vented three times. After repressurizing with ethylene (100 psi), the apparatus was heated to 100 °C for 24 h, while the reaction mixture was stirred using a magnetic stir plate. The bomb was then vented and the contents of the round-bottom flask were diluted with Et$_2$O and filtered to remove colorless crystals of NEt$_3$Br. The filtrate was purified by flash chromatography (hexanes) to yield 235 mg (90%) of clear colorless crystals. ^{1}H NMR (CDCl$_3$): 6.80 (dd, $J = 17.4$, 10.9 Hz, 2 H); 6.64 (dd, $J = 7.7$, 1.8 Hz, 2 H); 6.54 (d, $J = 1.8$ Hz, 2 H); 6.31 (d, $J = 7.7$ Hz, 2 H); 5.51 (dd, $J = 17.4$, 1.4 Hz, 2 H); 5.27 (dd, $J = 10.9$, 1.4 Hz, 2 H); 3.45 (m, 2 H); 3.1−2.9 (m, 4 H); 2.8 (m, 2 H). Calcd for C$_{20}$H$_{20}$: C, 92.3; H, 7.7. Found: C, 91.58; H, 7.82.

**4,12-Divinyl[2.2]paracyclophane (6b).** A 50-mL round-bottom flask charged with a Teflon-coated stir bar, 4,16-dibromoparacyclophane (500 mg, 1.37 mmol), Pd(OAc)$_2$ (12 mg, 0.05 mmol), tris(*o*-tolyl)-phosphine (81 mg, 0.27 mmol), triethylamine (2 mL) and DMF (9 mL) was placed into a high-pressure steel bomb containing a thin (2 cm) layer of sand. The round-bottom flask was fitted with a rubber septum and vented with a short 18 gauge needle. The bomb was then sealed and pressurized with ethylene (100 psi) and vented three times. After repressurizing with ethylene (100 psi), the vessel was heated to 100 °C for 23 h, while the reaction mixture was stirred using a magnetic stirring plate. The bomb was then vented and the contents of the round-bottom flask were diluted with water to precipitate the crude product. The solid was filtered off and rinsed with water, then dissolved in chloroform and filtered into a clean flask and dried (MgSO$_4$). Purification by flash chromatography (hexanes) yields 346 mg (97%) of white microcrystals. ^{1}H NMR (CDCl$_3$): 6.80 (br s, 2 H); 6.76 (dd, $J = 17.5$, 11.0 Hz, 2 H); 6.49 (br s, 4 H); 5.54 (dd, $J = 17.4$, 1.3 Hz, 2 H); 5.25 (dd, $J = 11$, 1.3 Hz, 2 H); 3.51 (m, 2 H); 3.13 (m, 2 H); 2.90−2.73 (m, 6 H). ^{13}C{^{1}H} NMR (CDCl$_3$): 139.6, 137.5, 137.2 (quat.), 134.9, 134.5, 131.9, 126.7, 114.0, 34.1, 33.9. Calcd for C$_{20}$H$_{20}$: C, 92.3; H, 7.7. Found: C, 91.82; H, 7.88.

**4-Styryl[2.2]paracyclophane (7).** A 25-mL round-bottom flask was charged with a Teflon-coated stir bar, 4-bromoparacyclophane (212 mg, 0.74 mmol), Pd(OAc)$_2$ (5 mg, 0.022 mmol), NBu$_4$Cl (213 mg, 0.77 mmol), K$_2$CO$_3$ (274 mg, 1.98 mmol), styrene (0.2 mL, 1.75 mmol), and DMF (8 mL). After fitting with a Kontes valve vacuum line adapter, the flask was evacuated and back-filled with nitrogen three times. The reaction mixture was then heated at 100 °C for 23 h with

(56) Burger, B. J.; Bercaw, J. E. In *Experimental Organometallic Chemistry*; Wayda, A. L., Darrensbourg, M. Y., Eds.; ACS Symp. Ser. 357; American Chemical Society: Washington, DC, 1987.

(57) Eaton, D. F. *Pure Appl. Chem.* **1988**, *60*, 1107.
(58) Khan, M. I.; Renak, M. L.; Bazan, G. C.; Popovic, Z. *J. Am. Chem. Soc.* **1997**, *119*, 5344.

stirring. The cooled reaction mixture was diluted with Et$_2$O (20 mL) and extracted with water (8 × 5 mL). The organic layer was then dried (MgSO$_4$) and purified by flash chromatography (hexanes) to yield 172 mg (75%) of colorless crystals. A single-crystal X-ray diffraction experiment was carried out on one of these. $^1$H NMR (CDCl$_3$): 7.58 (d, $J = 7$ Hz, 2 H, $o$-phenyl); 7.41 (t, $J = 7.4$ Hz, 2 H, $m$-phenyl); 7.30 (t, $J = 7.3$ Hz, 1 H, $p$-phenyl); 7.20, 6.90 (AB spin system, $J = 16$ Hz, 1 H each, vinyl); 6.71 (dd, $J = 7.8, 1.8$ Hz, 1 H); 6.67 (d, $J = 1.4$ Hz, 1 H); 6.55−6.43 (m, 5 H); 3.60 (m, 1 H); 3.17−2.81 (m, 7 H). $^{13}$C-{$^1$H} NMR (CDCl$_3$): 139.9, 139.4, 139.3, 138.4, 137.9, 137.4 (quat.), 135.0, 133.0, 131.8, 131.75, 130.2, 129.8, 129.2, 128.8, 127.5, 126.9, 126.5, 35.5, 35.3, 34.9, 34.0. Calcd for C$_{24}$H$_{22}$: C, 92.9; H, 7.1. Found: C, 92.97; H, 6.99.

**4,16-Distyryl[2.2]paracyclophane (1a).** A 100-mL round-bottom flask was charged with a Teflon-coated stir bar, 4,16-dibromoparacyclophane (323 mg, 0.88 mmol), styrene (0.3 mL, 2.6 mmol), triethylamine (2 mL), and DMF (25 mL). The reaction flask was fitted with a Kontes vacuum line adapter and evacuated and back-filled with nitrogen three times. This was transferred into an inert atmosphere glovebox, where Pd(OAc)$_2$ (4 mg, 0.018 mmol) and tris($o$-tolyl)-phosphine (21 mg, 0.07 mmol) were added to the flask. The flask was then fitted with a septum (secured with wire) and heated to 100 °C for 2 days while stirring. The cooled reaction mixture was diluted with water to afford a tan precipitate, which was filtered off and rinsed with water. The solid was dissolved in chloroform, filtered into a clean flask, and dried (MgSO$_4$). After filtering off the MgSO$_4$, the chloroform solution was reduced in volume and layered with hexanes to afford 171 mg (47%) of colorless crystals upon standing overnight. $^1$H NMR (CDCl$_3$): 7.57 (d, $J = 7.2$ Hz, 2 H, $o$-phenyl); 7.40 (t, $J = 7.4$ Hz, 2 H, $m$-phenyl); 7.28 (t, $J = 7.4$ Hz, 1 H, $p$-phenyl); 7.21, 6.87 (AB spin system, $J = 16.1$ Hz, 1 H each, vinyl); 6.68−6.61 (m, 2 H); 6.40 (d, $J = 7.7$ Hz, 1 H); 3.59 (m, 1 H); 3.11 (m, 1 H); 3.03−2.89 (m, 2 H). $^{13}$C{$^1$H} NMR (CDCl$_3$): 139.5, 138.2, 137.9, 137.4 (quat.), 133.6, 130.2, 129.5, 129.3, 128.7, 127.5, 127.0, 126.5, 34.5, 33.3. HREI Calcd for C$_{32}$H$_{28}$ = 412.2191. Found 412.2187. Calcd for C$_{32}$H$_{28}$: C, 93.2; H, 6.8. Found: C, 92.26; H, 6.59.

**4,12-Distyryl[2.2]paracyclophane (1b).** A 50-mL round-bottom flask was charged with a Teflon-coated stir bar, 4,12-dibromoparacyclophane (252 mg, 0.69 mmol), styrene (0.2 mL, 1.75 mmol), triethylamine (2 mL), and DMF (10 mL). The reaction flask was fitted with a Kontes vacuum line adapter and evacuated and back-filled with nitrogen three times. This was transferred into an inert atmosphere glovebox, where Pd(OAc)$_2$ (3 mg, 0.013 mmol) and P($o$-tol)$_3$ (15 mg, 0.049 mmol) were added to the flask. The flask was then fitted with a septum (secured with wire) and heated to 100 °C for 2 days with stirring. The cooled reaction mixture was filtered through Celite and diluted with chloroform. The solution was extracted with water (5 × 10 mL) and then dried (MgSO$_4$). After removing the volatiles under vacuum, the crude product was purified by flash chromatography (5:1 hexanes:chloroform) to afford 130 mg (46%) of colorless crystals. These can be recrystallized from warm pentane to obtain X-ray quality single crystals. $^1$H NMR (CDCl$_3$): 7.46 (d, $J = 7.6$ Hz, 2 H, $o$-phenyl); 7.38 (t, $J = 7.9$ Hz, 2 H, $m$-phenyl); 7.29 (t, $J = 7.3$ Hz, 1 H, $p$-phenyl); 7.22, 6.87 (AB spin system, $J = 16.2$ Hz, 1 H each, vinyl); 6.93 (d, $J = 1.5$ Hz, 1 H); 6.56 (d, second order, $J = 7.8$ Hz, 1 H); 6.52 (dd, second order, $J = 7.9, 1.5$ Hz, 1 H); 3.64 (m, 1 H); 3.18 (m, 1 H); 2.97−2.84 (m, 2 H). $^{13}$C{$^1$H} NMR (CDCl$_3$): 139.7, 138.0, 137.7, 136.8 (quat), 135.0, 131.8, 128.7, 127.5, 126.7, 126.6, 125.9, 34.5, 34.0. Calcd for C$_{32}$H$_{28}$: C, 93.2; H, 6.8. Found: C, 93.13; H, 6.91.

**2,5-Dimethylstilbene (1c).** A 10-mL pear-shaped flask was charged with a Teflon-coated stir bar, 2-bromo-$p$-xylene (0.37 mL, 1.49 mmol), styrene (0.37 mL, 3.22 mmol), and triethylamine (5 mL). The flask was fitted with a Kontes vacuum line adapter and evacuated and then back-filled with nitrogen three times. The sealed assembly was transferred into an inert atmosphere glovebox, where Pd(OAc)$_2$ (6 mg, 0.027 mmol) and P($o$-tol)$_3$ (32 mg, 0.11 mmol) were added to the reaction mixture. The flask was fitted with a rubber septum (secured with wire) and then heated to 100 °C with stirring for 12 h. The cooled reaction mixture was diluted with Et$_2$O, and the insoluble triethylammonium bromide was filtered off. The mass of triethylammonium bromide isolated (263 mg, 53%) and GC/MS analysis of the crude

reaction mixture indicated that only approximately half of the 2-bromoparaxylene starting material had been consumed. Purification by flash chromatography (3:1 hexanes/chloroform) affords 136 mg (24%) of white crystals following crystallization in the freezer overnight.

**Bis-4,16-(4-carboxaldehyde-styryl)[2.2]paracyclophane (8).** Work was performed in an inert atmosphere glovebox. A 25-mL round-bottom flask was charged with a Teflon-coated stir bar, 4,16-divinyl-[2.2]paracyclophane (123 mg, 0.47 mmol), 4-bromobenzaldehyde (177 mg, 0.96 mmol), Pd(OAc)$_2$ (3 mg, 0.013 mmol), NBu$_4$Br (317 mg, 0.98 mmol), K$_2$CO$_3$ (149 mg, 1.08 mmol), and dimethylacetamide (6 mL). The resulting reaction mixture was heated for 2 days with stirring at 105 °C. The crude product mixture was diluted with water and filtered. A gray solid was collected and washed with two portions (15 mL) of chloroform and then transferred to a 100-mL Erlenmeyer flask. The solid was warmed with 50 mL of chloroform and filtered hot. The solid which remained on the fritted funnel was extracted again with hot chloroform and repeated for a total of three extractions. The combined filtrate was reduced in volume on a rotary evaporator to obtain 96 mg (43%) of bright yellow crystals. $^1$H NMR (CDCl$_3$): 10.00 (s, 1 H, C$H$O); 7.90, 7.70 (AA′BB′ pattern, $J = 8$ Hz, 2 H each, aromatic); 7.37, 6.92 (AB pattern, $J = 16.0$ Hz, 1 H each, $trans$-alkene); 6.73 (d, $J = 1.5$ Hz, 1 H, cyclophane); 6.64 (dd, $J = 1.5, 7.8$ Hz, 1 H, cyclophane); 6.43 (d, $J = 7.7$ Hz, 1 H, cyclophane); 3.61, 3.15, 3.05−2.92 (m, 4 H total, C$H_2$). Calcd for C$_{34}$H$_{28}$O$_2$: C, 87.15; H, 6.02; O, 6.83. Found: C, 87.07; H, 5.92; O, 6.75.

**Bis-4,16-(4-vinyl-styryl)[2.2]paracyclophane (9).** A THF solution (10 mL) of the ylide reagent, CH$_2$PPh$_3$, was prepared upon dropwise addition of LDA (2.0 M, 0.28 mL, 0.56 mmol) to a slurry of CH$_3$-PPh$_3$Br (203 mg, 0.57 mmol) at 0 °C. This solution was allowed to stir for 1.5 h at 0 °C and was then transferred via cannula to a second THF slurry (10 mL) of bis-4,16-(4-carboxaldehyde-styryl)[2.2]-paracyclophane (80 mg, 0.17 mmol). The mixture was gradually warmed to ambient temperature and left to stir for 3 h upon which time the reaction was quenched by adding an aqueous NH$_4$Cl solution. The THF solvent was removed using a rotary evaporator and then chloroform was added and extracted with water (2 × 25 mL). The organic phase was collected and dried (MgSO$_4$) amd then purified by column chromatography (3:1 hexanes:chloroform) to yield 35 mg (42%) of bright lemon yellow microcrystals. $^1$H NMR (CDCl$_3$): 7.53, 7.44 (AA′BB′ pattern, $J = 8.3$ Hz, 2 H each, aromatic); 7.21, 6.86 (AB pattern, $J = 16.2$ Hz, 1 H each, $trans$-alkene); 6.73 (dd, $J = 10.9, 17.6$ Hz, 1 H, vinyl); 6.67 (d, $J = 1.6$ Hz, 1 H, cyclophane); 6.63 (dd, $J = 1.7, 7.7$ Hz, 1 H, cyclophane); 6.40 (d, $J = 7.7$ Hz, 1 H, cyclophane); 5.78 (dd, $J = 0.7, 17.6$ Hz, 1 H, vinyl); 5.26 (dd, $J = 0.7, 10.9$ Hz, 1 H, vinyl); 3.59, 3.11, 3.01, 2.94 (m, 1 H each, C$H_2$). $^{13}$C{$^1$H} NMR (CDCl$_3$): 139.5, 138.2, 137.5, 137.3, 136.8 (quaternary), 136.4, 133.6, 130.1, 129.5, 128.9, 126.9, 126.64, 126.61, 113.7 (aromatic and vinyl), 34.5, 33.4 (CH$_2$). Calcd. for C$_{36}$H$_{32}$: C, 93.06; H, 6.94. Found: C, 92.95; H, 6.77.

***p*-Vinylbenzylphosphonium Chloride.** A toluene (50 mL) solution of *p*-vinylbenzyl chloride (90%, 8.7 g, 51.3 mmol) and triphenylphosphine (13.1 g, 49.9 mmol) was heated with stirring to 110 °C for 12 h. The resulting white crystalline solid was filtered off and washed with toluene and then dried under vacuum. Yield 12.6 g (61%). $^1$H NMR (CDCl$_3$): 7.74 (m, 9H, PPh$_3$); 7.60 (m, 6 H, PPh$_3$); 7.12, 7.04 (AA′BB′ pattern, $J = 8$ Hz, 2 H each, aromatic); 6.57 (dd, $J = 10.9$ and 17.4 Hz, 1 H, vinyl); 5.65 (d, $J = 17.5$ Hz, 1 H, vinyl); 5.52 (d, $J_{PH} = 14.7$ Hz, 2 H, benzylic); 5.20 (d, $J = 10.8$ Hz, 1 H, vinyl).

***trans*-4,4′-*tert*-Butylvinylstilbene.** To an Et$_2$O suspension/solution of *p*-vinylbenzylphosphonium chloride (3.99 g, 9.6 mmol) and 4-*tert*-butylbenzaldehyde (1.7 mL, 10.1 mmol) was added LiOEt (1.0 M in EtOH, 10 mL) dropwise over 30 min. The resulting homogeneous solution was extracted with water and brine and then dried over MgSO$_4$. The crude product mixture was purified by column chromatography (hexanes). The initial fractions containing the *cis* isomer were combined and heated with a small amount of I$_2$ to catalyze the isomerization to the desired *trans* isomer. The later fractions containing pure *trans* isomer were then combined with the isomerized fractions to afford 1.93 g (77%) of product. $^1$H NMR (CDCl$_3$): 7.45, 7.38 (AA′BB′ pattern, 4 H each, aromatic); 7.09, 7.03 (AB pattern, 2H, $J = 16.4$ Hz); 6.70

*Stilbenoid Dimers*

*J. Am. Chem. Soc., Vol. 120, No. 36, 1998*  9203

(dd, $J$ = 10.8, 17.6 Hz, 1H, vinyl); 5.74 (dd, $J$ = 0.8, 17.6 Hz, 1 H); 5.22 (dd, $J$ = 0.8, 10.9 Hz, 1 H, vinyl); 1.32 (s, 9 H, *tert*-butyl).

**4-(4′-*tert*-Butylstyryl)styryl[2.2]paracyclophane (10).** A 25-mL round-bottom flask was charged with a Teflon-coated stir bar, 4-bromoparacyclophane (175 mg, 0.61 mmol), Pd(OAc)₂ (14 mg, 0.062 mmol), NBu₄Cl (290 mg, 1.04 mmol); K₂CO₃ (250 mg, 1.81 mmol), 4,4′-*tert*-butylvinylstilbene (158 mg, 0.602 mmol), and DMF (7 mL). After fitting with a Kontes valve vacuum line adapter, the flask was evacuated and back-filled with nitrogen three times. The reaction mixture was then heated at 100 °C for 1 day with stirring. The cooled reaction mixture was diluted with CHCl₃ (100 mL) and extracted with water (8 × 20 mL). The organic phase was then dried (MgSO₄) and purified by flash chromatography (hexanes) to yield 149 mg (53%) of bright fluorescent yellow powder. ¹H NMR (CDCl₃): 7.55, 7.52 (second order AA′BB′ pattern, $J$ = 9 Hz, 4 H, 1,4-substituted arene); 7.47, 7.39 (AA′BB′ pattern, $J$ = 8 Hz, 2 H each, 1,4-substituted arene); 7.19, 6.88 (AB pattern, $J$ = 16.2 Hz, 1 H each, *trans*-alkene); 7.14, 7.08 (AB pattern, $J$ = 16.4 Hz, 1 H each, *trans*-alkene); 6.69 (dd, $J$ = 1.8, 7.9 Hz, 1 H, paracyclophane); 6.66 (d, $J$ = 1.3 Hz, 1 H, paracyclophane); 6.56−6.42 (overlapping multiplets, 5 H, paracyclophane); 3.59 (m, 2 H, C$H_2$); 3.19−2.78 (overlapping multiplets, 6 H, C$H_2$); 1.34 (s, 9 H, *tert*-butyl). ¹³C{¹H} NMR (CDCl₃): 150.9, 139.9, 139.34, 139.27, 138.4, 137.4, 137.1, 136.9, 134.6 (quaternary), 135.0, 133.0, 131.8, 131.7, 130.1, 129.9, 128.8, 128.4, 127.5, 126.8, 126.7, 126.3, 125.7 (aromatic), 35.5, 35.3, 34.9, 34.0 (*C*H₂), 34.7 (*C*Me₃), 31.3 (C*Me*₃). Calcd for C₃₆H₃₆: C, 92.3; H, 7.7. Found: C, 91.82; H, 7.97.

**4,16-Bis[4-(4′-*tert*-butylstyryl)styryl][2.2]paracyclophane(2a).** A 25-mL round-bottom flask was charged with a Teflon-coated stir bar, 4,16-dibromoparacyclophane (108 mg, 0.295 mmol), 4,4′-*tert*-butylvinylstilbene (154 mg, 0.59 mmol), Pd(OAc)₂ (3 mg, 0.013 mmol), tris-(*o*-tolyl)phosphine (16 mg, 0.053 mmol), triethylamine (1 mL), and DMF (5 mL). The flask was fitted with a Kontes vacuum line adapter and then evacuated and back-filled with nitrogen three times. The sealed assembly was then heated to 100 °C with stirring for 2 days. The cooled reaction mixture was diluted with water to afford a yellow precipitate, which was filtered off and rinsed with water. The solid was dissolved in chloroform and filtered into a clean flask and then dried (MgSO₄). Purification by flash chromatography (hexanes/chloroform) yields 82 mg (38%) of bright fluorescent yellow powder. ¹H NMR (CDCl₃): 7.56, 7.53 (second-order AA′BB′, $J$ = 8.8 Hz, 4 H, phenyl); 7.47, 7.39 (AA′BB′, $J$ = 8.5 Hz, 4 H, phenyl); 7.22, 6.88 (AB spin system, $J$ = 16.0 Hz, 2 H, vinyl); 7.14, 7.09 (AB spin system, $J$ = 16.2 Hz, 2 H, vinyl); 6.69 (d, $J$ = 1.8 Hz, 1 H); 6.65 (dd, $J$ = 7.7, 1.8 Hz, 1H); 6.41 (d, $J$ = 7.7 Hz, 1 H); 3.61 (m, 1H); 3.12 (m, 1 H); 3.04−2.88 (m, 2 H); 1.33 (s, 9 H). ¹³C{¹H} NMR (CDCl₃): 150.9, 139.5, 138.2, 137.4, 137.1, 136.9, 134.6, 133.6, 130.1, 129.5, 128.9, 128.4, 127.5, 126.8, 126.3, 125.7, 34.6, 34.5, 33.4, 31.3. HREI Calcd for C₅₆H₅₆: 729.12. Found: 728.44. Calcd for C₅₆H₅₆: C, 92.2; H, 7.7. Found: C, 92.06; H, 7.73.

**4,12-Bis[4-(4′-*tert*-butylstyryl)styryl][2.2]paracyclophane (2b).** A 25-mL round-bottom flask was charged with a Teflon-coated stir bar, 4,12-dibromoparacyclophane (102 mg, 0.28 mmol), 4,4′-*tert*-butylvinylstilbene (147 mg, 0.56 mmol), Pd(OAc)₂ (3.3 mg, 0.015 mmol), tris(*o*-tolyl)phosphine (18 mg, 0.059 mmol), triethylamine (1 mL), and DMF (5 mL). The flask was fitted with a Kontes vacuum line adapter and then evacuated and back-filled with nitrogen three times. The sealed assembly was then heated to 100 °C with stirring for 2 days. The cooled reaction mixture was diluted with water to afford a yellow precipitate, which was filtered off and rinsed with water. The solid was dissolved in chloroform and filtered into a clean flask and then dried (MgSO₄). Purification by flash chromatography (hexanes/chloroform) yields 65 mg (32%) of bright fluorescent yellow powder. ¹H NMR (CDCl₃): 7.53, 7.45 (second-order AA′BB′, $J$ = 8.3 Hz, 4 H, phenyl); 7.49, 7.39 (second-order AA′BB′, $J$ = 8.4 Hz, 4 H, phenyl); 7.21, 6.87 (AB spin system, $J$ = 16.3 Hz, 2 H, vinyl); 7.17, 7.11 (AB spin system, $J$ = 16.3 Hz, 2 H, vinyl); 6.94 (d, $J$ = 1.4 Hz, 1 H); 6.54 (d, $J$ = 7.8 Hz, 1 H); 6.50 (dd, $J$ = 7.8, 1.4 Hz, 1 H); 3.64 (m, 1 H); 3.18 (m, 1 H); 2.96−2.83 (m, 2 H); 1.34 (s, 9 H, *tert*-butyl). ¹³C{¹H} NMR (CDCl₃): 150.9, 145.9, 139.7, 138.0, 136.9, 136.8, 135.0, 134.6, 131.8,

128.4, 128.3, 127.6, 126.9, 126.8, 126.6, 126.3, 125.7, 34.7, 34.5, 34.1, 31.3. Calcd for C₅₆H₅₆: C, 92.2; H, 7.7. Found: C, 91.42; H, 7.85.

**4-(2,5-Dimethylstyryl)-4′-*tert*-butylstilbene (2c).** A 25-mL round-bottom flask charged with 4,4′-*tert*-butylvinylstilbene (0.1 g, 0.38 mmol), 2-bromo-*p*-xylene (0.085 g, 0.46 mmol), Pd(OAc)₂ (7 mg, 0.0031 mmol), tris(*o*-tolyl)phosphine (12 mg, 0.0034 mmol), triethylamine (3 mL), and DMF (5 mL) was heated to 120 °C for 2 days. The crude reaction mixture was poured into water and extracted with chloroform. The volatiles were stripped under vacuum, and the residue purified by flash chromatography (hexanes/chloroform) to give 82 mg (60%) of product. ¹H NMR (CDCl₃): 7.50 (s, 4 H, aromatic); 7.46, 7.38 (AA′BB′ pattern, $J$ = 6.6 Hz, 2 H each, aromatic); 7.42 (br s, 1 H, aromatic); 7.32, 6.98 (AB pattern, $J$ = 16.1 Hz, 1 H each, *trans*-alkene); 7.11, 7.06 (AB pattern, $J$ = 16.3 Hz, 1 H each, *trans*-alkene); 7.06 (d, $J$ = 8 Hz, 1 H, aromatic); 6.99 (br d, $J$ = 8 Hz, 1 H, aromatic); 2.39, 2.35 (s, 3 H each, methyl); 1.33 (s, 9 H, *tert*-butyl). ¹³C{¹H} NMR (CDCl₃): 150.8, 136.9, 136.8, 136.1, 135.5, 134.6, 132.8 (quat), 130.4, 129.3, 128.36, 128.35, 127.5, 126.8, 126.7, 126.4, 126.2, 125.9, 125.6, 34.7, 31.3, 21.1, 19.5.

**X-ray Diffraction Structure Determination of 4b.** Single crystals of **2b** (C₁₆H₁₄Br₂; FW = 366.09) were grown upon slow diffusion of hexanes into a concentrated CHCl₃ solution. A colorless fragment of approximate dimensions 0.08 × 0.10 × 0.22 mm³ was separated from a collection of crystals under Paratone-8277, mounted under oil on a glass fiber, and immediately placed in a cold nitrogen stream at −80 °C on the X-ray diffractometer. The X-ray intensity data were collected on a standard Siemens SMART CCD Area Detector System equipped with a normal focus molybdenum target X-ray tube operated at 2.0 kW (50 kV, 40 mA). A total of 1321 frames of data (1.3 hemispheres) were collected using a narrow frame method with scan widths of 0.3° in ω and exposure times of 10 s/frame using a detector-to-crystal distance of 5.094 cm (maximum 2θ angle of 45°). The total data collection time was approximately 6 h. Frames were integrated with the Siemens SAINT program to yield a total of 4219 reflections, of which 1768 were independent ($R_{int}$ = 3.85%, $R_{sig}$ = 5.61%) and 1609 were above 2σ($I$). The unit cell parameters (at −80 °C) of $a$ = 12.2397-(6) Å and $c$ = 7.8363(5) Å were based upon the least-squares refinement of three-dimensional centroids of 2618 reflections. The space group was assigned as $P3_1$ ($Z$ = 3) on the basis of systematic absences by using the XPREP program (Siemens, SHELXTL 5.04). The structure was solved by using direct methods and refined by full-matrix least-squares on $F^2$. All non-hydrogen atoms were refined anisotropically with hydrogen atoms included in idealized positions giving a data/parameter ratio of approximately 11:1. The structure refined to a goodness of fit (GOF) of 1.002 and final results of $R_1$ = 3.97% ($I$ > 2σ($I$)), $wR_2$ = 8.54% ($I$ > 2σ($I$)).

**X-ray Diffraction Structure Determination of 7.** Single crystals of **7** (C₂₄H₂₂ FW = 310.42) were grown from hexanes. A colorless fragment of approximate dimensions 0.38 × 0.28 × 0.26 mm was cut from a large block-shaped single crystal under Paratone-8277, mounted under oil on a glass fiber, and immediately placed in a cold nitrogen stream at −80 °C on the X-ray diffractometer. The X-ray intensity data were collected on a standard Siemens SMART CCD Area Detector System equipped with a normal focus molybdenum-target X-ray tube operated at 2.0 kW (50 kV, 40 mA). A total of 1321 frames of data (1.3 hemispheres) were collected using a narrow frame method with scan widths of 0.3° in ω and exposure times of 60 s/frame using a detector-to-crystal distance of 5.094 cm (maximum 2θ angle of 56.52°). The total data collection time was ~24 h. Frames were integrated with the Siemens SAINT program to yield a total of 9529 reflections, of which 3782 were independent ($R_{int}$ = 2.64%, $R_{sig}$ = 3.83%) and 2727 were above 2σ($I$). The unit cell parameters (at −80 °C) of $a$ = 19.5096-(6) Å, $b$ = 11.2834(3) Å, and $c$ = 7.7184(2) Å, and $β$ = 97.804(1) were based upon the least-squares refinement of three-dimensional centroids of 4256 reflections. The space group was assigned as $P2_1/c$ ($Z$ = 4) on the basis of systematic absences by using the XPREP program (Siemens, SHELXTL 5.04). The structure was solved by using direct methods and refined by full-matrix least-squares on $F^2$. All non-hydrogen atoms were refined anisotropically with hydrogen atoms included in idealized positions giving a data/parameter ratio of

approximately 16:1. The structure refined to a goodness of fit (GOF) of 1.050 and final results of $R_1 = 5.11\%$ ($I > 2\sigma(I)$), $wR_2 = 12.26\%$ ($I > 2\sigma(I)$).

**Supporting Information Available:** Complete experimental details the X-ray crystallographic determination of **4b** and **7** (16 pages). See any current masthead page for ordering information and Web access instructions.

JA973816H